# A well-balanced conservative high-order alternative finite difference WENO (A-WENO) method for Euler equations with gravity

Yuanzhe Wei[1], Ziyao Xu[2], and Chi-Wang Shu*[3]

[1]Division of Applied Mathematics, Brown University, Providence, RI 02912, USA. E-mail: yuanzhe_wei@brown.edu

[2]Department of Mathematics and Statistics, Binghamton University, Vestal, NY 13902, USA. E-mail: zxu24@binghamton.edu

[3]Division of Applied Mathematics, Brown University, Providence, RI 02912, USA. E-mail: chi-wang_shu@brown.edu.

**Abstract**

We develop a conservative, high-order well-balanced alternative finite difference weighted essentially non-oscillatory (A-WENO) method for the Euler equations with gravitational source terms. The method is designed to exactly preserve isentropic hydrostatic and non-hydrostatic steady states. The well-balanced property is achieved by reformulating the source terms using local reference equilibrium states and by interpolating equilibrium variables, which remain constant at steady state, in the construction of the numerical fluxes. The A-WENO framework enables high-order accuracy while maintaining conservation. The method is extended to multidimensional Euler equations in Cartesian and spherical coordinates. Numerical experiments demonstrate the designed high-order accuracy, exact preservation of steady states up to round-off errors, and accurate resolution of small perturbations around equilibria.

*Keywords: Euler equations, well-balanced, A-WENO*

## 1 Introduction

The Euler equations with gravitational source terms arise in a wide range of applications in fluid dynamics and astrophysics, including atmospheric flows, stellar dynamics, accretion processes, and astrophysical gas dynamics. In any number of space dimensions, the Euler equations can be written in conservative form as

$$\frac{\partial}{\partial t}\begin{pmatrix}\rho\\ \mathbf{m}\\ E\end{pmatrix}+\nabla\cdot\begin{pmatrix}\mathbf{m}\\ \rho\mathbf{u}\otimes\mathbf{u}+p\mathbf{I}\\ (E+p)\mathbf{u}\end{pmatrix}=\begin{pmatrix}0\\ -\rho\nabla\Phi\\ -\mathbf{m}\cdot\nabla\Phi\end{pmatrix},\qquad t>0, \tag{1}$$

where $\rho$ is the density, $\mathbf{m}=\rho\mathbf{u}$ is the momentum, $\mathbf{u}$ is the velocity, $E$ is the total energy per unit volume, $p$ is the pressure, and $\Phi$ is the prescribed gravitational potential. For an ideal gas,

$$E=\frac{1}{2}\rho|\mathbf{u}|^2+\frac{p}{\gamma-1},$$

where $\gamma>1$ is the ratio of specific heats.

The Euler equations with gravity constitute an important example of hyperbolic balance laws. Due to the presence of the source terms, they admit nontrivial steady-state solutions $(\rho_e,\mathbf{m}_e,E_e)$, or

*Research supported in part by NSF grant DMS-2309249.

*equilibria*, which are solutions independent of $t$. In particular, such solutions for Euler equations (1) satisfy

$$\nabla \cdot \begin{pmatrix} \mathbf{m_e} \\ \rho_e \mathbf{u_e} \otimes \mathbf{u_e} + p_e \mathbf{I} \\ (E_e + p_e)\mathbf{u_e} \end{pmatrix} = \begin{pmatrix} 0 \\ -\rho_e \nabla \Phi \\ -\mathbf{m_e} \cdot \nabla \Phi \end{pmatrix}. \tag{2}$$

Standard numerical methods, however, do not generally satisfy (2) at the discrete level. As a result, even when the exact solution is an equilibrium state, truncation errors may generate spurious numerical perturbations. This issue is particularly significant when the physical solution is a small perturbation of an equilibrium, since the numerical errors caused by the imbalance may be comparable to or even larger than the perturbation of interest. Well-balanced numerical methods are designed to overcome this difficulty by exactly preserving certain equilibrium states at the discrete level.

The development of well-balanced schemes dates back to the works of Cargo and LeRoux [1] and Greenberg and LeRoux [5]. LeVeque [12] subsequently developed the quasi-steady wave-propagation approach for balancing source terms and flux gradients. Since then, well-balanced methods have been extensively studied for a variety of hyperbolic balance laws; see, for example, the recent review [9] and the references therein.

A prototypical model for the development of well-balanced methods is the shallow water system with non-flat bottom topography. Much of the early work focused on the lake-at-rest equilibrium. The preservation of moving-water equilibria, for which the velocity does not vanish, is considerably more challenging. High-order finite volume WENO schemes preserving moving-water equilibria were developed in [15], while Cheng and Kurganov [4] constructed a moving-water equilibria preserving central-upwind method based on the reconstruction of equilibrium variables. Exactly well-balanced DG methods for moving-water equilibria have also been developed; see, for example, [21]. More generally, Parés and Parés-Pulido [16] proposed a framework for constructing well-balanced high-order finite difference methods for systems of balance laws.

Well-balanced methods for the Euler equations with gravitational fields have also received considerable attention. Most of the earlier works focused on hydrostatic equilibria, in which case $\mathbf{u}_e = \mathbf{0}$. Käppeli and Mishra [10] developed well-balanced finite volume schemes for the Euler equations with gravity. High-order finite volume methods were subsequently studied in [11]. High-order finite difference WENO schemes for gas dynamics under gravitational fields were developed by Xing and Shu [22] and Li and Xing [14]. Within the discontinuous Galerkin framework, well-balanced methods for the Euler equations with gravity have been developed in, for example, [3, 13, 20].

Compared with hydrostatic equilibria, well-balanced methods for steady flows with nonzero velocity, namely $\mathbf{u}_e \neq \mathbf{0}$, have received less attention and are more difficult to construct. It follows from (2) that, for a steady isentropic flow, the entropy parameter and Bernoulli quantity

$$s = \frac{p}{\rho^\gamma}, \qquad Q = \frac{1}{2}|\mathbf{u}|^2 + \frac{\gamma}{\gamma - 1}\frac{p}{\rho} + \Phi \tag{3}$$

are constant along streamlines. In one space dimension, the mass flux is also constant, so that the steady state can be characterized by

$$(m, s, Q) = \left(\rho u, \frac{p}{\rho^\gamma}, \frac{1}{2}u^2 + \frac{\gamma}{\gamma - 1}\frac{p}{\rho} + \Phi\right) = \text{constant}.$$

These are called the equilibrium variables, which will be studied in detail in Section 2.4. The hydrostatic isentropic equilibrium is included as the special case $m = 0$.

Grosheintz-Laval and Käppeli [6] developed well-balanced finite volume schemes based on local steady-state reconstruction for steady isentropic flows. Although their method is at most second order accurate, it preserves non-hydrostatic equilibria and is applicable to continuous subsonic and supersonic steady flows. With a numerical flux capable of exactly resolving stationary discontinuities, the

method can also preserve steady states containing stationary shocks located at cell interfaces, in which case the quantity $s$ experiences a jump across the shock, so the flow is not isentropic but only adiabatic. More recently, Xu and Shu [23] developed a high-order well-balanced DG method for general non-hydrostatic equilibria of the shallow water and Euler equations. The source term is reformulated in terms of the flux gradient of a local reference equilibrium state and discretized using Gauss–Lobatto quadrature in the same manner as the flux integral, thereby producing an exact discrete balance at equilibrium.

The construction of conservative high-order well-balanced finite difference schemes introduces an additional difficulty. In low-order methods, point values at cell centers and cell averages can often be used interchangeably without affecting the designed order of accuracy. This is no longer true for high-order methods. In [24], Xu and Shu developed a conservative high-order alternative finite difference WENO (A-WENO) method for the shallow water equations with non-flat bottom topography. The source term is reformulated into a flux-gradient form and discretized consistently with the true flux gradient. In addition, the equilibrium variables, which remain constant at steady states, are interpolated in the construction of the numerical flux. Since the A-WENO framework operates directly on point values, it provides a natural way to construct high-order well-balanced schemes based on equilibrium variables while maintaining the conservation property.

In this paper, we extend the well-balanced A-WENO framework of [24] to the Euler equations with gravitational source terms. The extension is nontrivial because the transformation between the conservative and equilibrium variables is nonlinear and depends on the flow regime, which may cause instability in complex transonic flows in higher dimensions. For example, in one dimension, given the equilibrium variables $(m,s,Q)$, the density is determined implicitly by

$$\frac{1}{2}\frac{m^2}{\rho^2}+\frac{\gamma s}{\gamma-1}\rho^{\gamma-1}+\Phi=Q. \tag{4}$$

For suitable values of $(m,s,Q)$, equation (4) may have two solutions corresponding to the subsonic and supersonic branches. Therefore, the flow regime must be taken into account when the conservative variables are recovered from the equilibrium variables, which is easy to do in 1D but becomes sensitive in higher dimensions.

Although the numerical method is first formulated for a general 1D system of hyperbolic balance laws (Sections 2.1–2.2), our main objective is to solve the Euler equations in 2D and 3D (Sections 2.3–2.4). We consider a class of isentropic equilibrium states that are one-dimensional in nature, namely, the equilibrium state and the gravitational potential vary only along one coordinate direction. This includes, for example, planar equilibria in Cartesian coordinates and radially symmetric equilibria in spherical coordinates. The method is formulated in detail in Cartesian coordinates as well as spherical coordinates.

The proposed method is conservative, high-order accurate, and exactly preserves the targeted isentropic steady states up to round-off errors. By performing WENO interpolation on suitably chosen equilibrium variables, the method preserves both hydrostatic and non-hydrostatic steady states and can treat different flow regimes. Numerical experiments verify the designed high-order accuracy and well-balanced property of the method in Cartesian and spherical coordinates. They also demonstrate that the proposed method accurately resolves small perturbations of equilibrium states on coarse meshes while maintaining robustness for solutions away from equilibrium.

The remainder of this paper is organized as follows. The discussion of our algorithm is contained in Section 2. In Sections 2.1–2.2, we first present the source-term reformulation and the well-balanced A-WENO method for general 1D hyperbolic balance laws and then discuss its multidimensional extension in Section 2.3. The construction of the equilibrium variables and their application to the Euler equations in Cartesian and spherical coordinates are presented subsequently in Section 2.4, and a local adaptation step is introduced in Section 2.5 to resolve the instability near transonic regions. In

Section 3, numerical experiments in 2D and 3D are provided to verify the high-order accuracy, robustness, well-balanced property, and capability of resolving small perturbations of steady states. Finally, concluding remarks are given in the last section.

# 2 Algorithm

Although our present work focuses on solving 2D and 3D Euler equations, the algorithm is best understood and easiest explained in 1D. In what follows, we shall first present the scheme for a general 1D system of balance laws, then show the straightforward extension to the $n$-dimensional system.

## 2.1 Reformulation of the source term in 1D

Consider a generic system of hyperbolic balance laws in one space dimension:

$$\mathbf{U}_t + \mathbf{F}(\mathbf{U})_x = \mathbf{S}(x, \mathbf{U}), \quad x \in \mathbb{R}, \tag{5}$$

where $\mathbf{U} = (u_1, \cdots, u_N)^T$, $\mathbf{F}(\mathbf{U}) = (f_1(\mathbf{U}), \cdots, f_N(\mathbf{U}))^T$ and $\mathbf{S}(x, \mathbf{U}) = (s_1(x, \mathbf{U}), \cdots, s_N(x, \mathbf{U}))^T$ are vectors in $\mathbb{R}^N$. Suppose $\mathbf{U}_e$ is an equilibrium state of the balance law (5) satisfying $\mathbf{F}(\mathbf{U}_e)_x = \mathbf{S}(x, \mathbf{U}_e)$ for all $x \in \mathbb{R}$, then we can rewrite (5) as follows:

$$\mathbf{U}_t + \mathbf{F}(\mathbf{U})_x = \mathbf{S}(x, \mathbf{U}) \frac{\mathbf{F}(\mathbf{U}_e)_x}{\mathbf{S}(x, \mathbf{U}_e)}, \quad x \in \mathbb{R}, \tag{6}$$

where the operation on the right-hand side is to be understood as component-wise. If some component of $\frac{\mathbf{F}(\mathbf{U}_e)_x}{\mathbf{S}(x,\mathbf{U}_e)}$, say the $i$th component $\frac{f_i(\mathbf{U}_e)_x}{s_i(x,\mathbf{U}_e)}$ is of the form $\frac{0}{0}$, then we set this quotient to 1. Now an important observation follows: the system (5) generally admits an infinite family of equilibrium states $\mathbf{U}_e$, and we may choose any particular one of them to form (6), since they all satisfy $\mathbf{F}(\mathbf{U}_e)_x = \mathbf{S}(x, \mathbf{U}_e)$ for all $x \in \mathbb{R}$. Directly based on the reformulation of the source term in (6), we can write our well-balanced semi-discrete finite difference scheme as follows:

$$\begin{aligned} \frac{\mathrm{d}\mathbf{U}_j}{\mathrm{d}t} + \frac{1}{\Delta x}\left(\hat{\mathbf{F}}(\mathbf{U}_{j-r+1}, \cdots, \mathbf{U}_{j+s}) - \hat{\mathbf{F}}(\mathbf{U}_{j-r}, \cdots, \mathbf{U}_{j+s-1})\right) = \frac{\mathbf{S}(x_j, \mathbf{U}_j)}{\mathbf{S}(x_j, \mathbf{U}_{e,j}(x_j))} \times \\ \frac{1}{\Delta x}\left(\hat{\mathbf{F}}(\mathbf{U}_{e,j}(x_{j-r+1}), \cdots, \mathbf{U}_{e,j}(x_{j+s})) - \hat{\mathbf{F}}(\mathbf{U}_{e,j}(x_{j-r}), \cdots, \mathbf{U}_{e,j}(x_{j+s-1}))\right), \end{aligned} \tag{7}$$

where if in the $i$th equation $s_i(x_j, \mathbf{U}_j) \equiv 0$, we set $\frac{s_i(x_j,\mathbf{U}_j)}{s_i(x_j,\mathbf{U}_{e,j}(x_j))} = 1$. In the scheme (7), $\mathbf{U}_j$ is the numerical solution that approximates $\mathbf{U}$ at the nodes $x_j = j\Delta x$, $\hat{\mathbf{F}} = (\hat{f}_1, \cdots, \hat{f}_N)^T$ is a high-order numerical flux that approximates $\mathbf{F}$ at the cell interfaces, and $\mathbf{U}_{e,j}$ is an equilibrium state that is constructed locally from the information near the node $x_j$, namely from the point values $\{\mathbf{U}_k\}_{k=j-r}^{j+s}$. Note that the function $\mathbf{U}_{e,j}(x)$ may be different for each $j$. We only require $\mathbf{U}_{e,j}$ to satisfy the following condition:

**(A)** For any fixed $j$, if $\{\mathbf{U}_k\}_{k=j-r}^{j+s}$ are the point values of an equilibrium state $\mathbf{U}_e(x)$ at points $x = x_k$, $k = j-r, \cdots, j+s$, then $\mathbf{U}_{e,j}(x)$ must coincide with $\mathbf{U}_e(x)$ at the points $x = x_k$ for all $k = j-r, \cdots, j+s$.

This condition can guarantee that the scheme exactly preserves the equilibria. As mentioned previously, one can use any particular equilibrium state in the reformulation (6). The idea here is that, there is generally a unique equilibrium state $\mathbf{U}_e(x)$ for $x \in \mathbb{R}$ such that $\mathbf{U}_e(x_j) = \mathbf{U}_j$ for any fixed $j$; let us call this special equilibrium state $\mathbf{U}_{e,j}(x)$ and use it in the right-hand side of (7). Then, whenever the initial condition $\mathbf{U}_j$ is an equilibrium state itself, $\mathbf{U}_k$ and $\mathbf{U}_{e,j}(x_k)$ would coincide for all $k$, and the finite differences on the left- and right-hand side of (7) would be exactly equal and cancel each

other, leaving $\frac{\mathrm{d}\mathbf{U}_j}{\mathrm{d}t} = 0$, so that the scheme becomes well-balanced. Also, the scheme has high-order accuracy if $\hat{\mathbf{F}}$ is a high-order numerical flux, since $\frac{\mathbf{F}(\mathbf{U}_e)_x}{\mathbf{S}(x,\mathbf{U}_e)} = 1$.

The above is the basic idea, but it has two problems:

**(1)** For those equations in the system (5) where the source term is identically zero (e.g. the continuity equation in Euler equations), the resulting scheme is not necessarily conservative.

**(2)** For a fixed $j$, there might not exist an equilibrium state $\mathbf{U}_e(x)$ such that $\mathbf{U}_e(x_j) = \mathbf{U}_j$.

In what follows we will resolve these two issues. In particular, to ensure the scheme is conservative, we need to pick a special numerical flux $\hat{\mathbf{F}}$. In the next step (Section 2.2) we would discuss how to design the $\hat{\mathbf{F}}$ by performing WENO interpolation on a specially chosen transformation of $\mathbf{U}_j$ such that it becomes conservative for the subsystem of conservation laws contained in the balance law (e.g. the continuity equation in Euler equations). In doing so, as we shall soon see, the computational costs in approximating the source term is also minimized. As for the second problem, we will demonstrate how to reconstruct $\mathbf{U}_{e,j}(x)$ based on the information near $x_j$ only for Euler equations in Section 2.4.

## 2.2 The well-balanced A-WENO method in 1D

In this section, we define the well-balanced A-WENO method in 1D. Suppose $\mathbf{U} \in \mathbb{R}^N$. In what follows, we assume that there exists a transformation $\mathbf{V} = \mathbf{V}(\mathbf{U},x) \in \mathbb{R}^N$ such that $\mathbf{V}(\mathbf{U},x)$ is constant throughout the physical space when $\mathbf{U}$ is in an equilibrium state. We call such $\mathbf{V}$ a vector of equilibrium variables. For the expressions of equilibrium variables of Euler equations used in this paper, see Section 2.4. For now, we assume that the transformation $\mathbf{U} \to \mathbf{V}(\mathbf{U},x)$ is invertible (which is technically not true for the equilibrium variables adopted in this paper; we will see how to resolve this issue in Section 2.4) and denote its inverse by $\mathbf{U} = \mathbf{U}(\mathbf{V},x)$. Let the one space dimension be discretized by a uniform grid with mesh size $\Delta x$ and denote by $I_j = [x_{j-\frac{1}{2}}, x_{j+\frac{1}{2}}]$ the $j$th cell centered at $x_j = j\Delta x$. In this paper, we only present the fifth-order scheme to illustrate the concept, in which case $r = s = 3$ in (7), but the method can be generalized to arbitrary high orders.

### 2.2.1 Fifth-order WENO interpolation

Assume that the point values

$$p_{j-2}, p_{j-1}, p_j, p_{j+1}, p_{j+2}$$

are available at the grid points $x_k$, where $k = j-2, \ldots, j+2$. The fifth-order WENO-JS interpolation [2, 8, 18] approximates the left limit value at the interface $x_{j+\frac{1}{2}}$ by

$$p^-_{j+\frac{1}{2}} = w_1 p^{-(1)}_{j+\frac{1}{2}} + w_2 p^{-(2)}_{j+\frac{1}{2}} + w_3 p^{-(3)}_{j+\frac{1}{2}}, \tag{8}$$

where the three candidate interpolants are

$$\begin{aligned} p^{-(1)}_{j+\frac{1}{2}} &= \frac{3}{8}p_{j-2} - \frac{5}{4}p_{j-1} + \frac{15}{8}p_j, \\ p^{-(2)}_{j+\frac{1}{2}} &= -\frac{1}{8}p_{j-1} + \frac{3}{4}p_j + \frac{3}{8}p_{j+1}, \\ p^{-(3)}_{j+\frac{1}{2}} &= \frac{3}{8}p_j + \frac{3}{4}p_{j+1} - \frac{1}{8}p_{j+2}. \end{aligned} \tag{9}$$

Each of these interpolants is constructed on a different three-point stencil. Their contributions are combined through the nonlinear weights $w_1, w_2, w_3 \geq 0$, defined by

$$w_k = \frac{\omega_k}{\sum_{m=1}^3 \omega_m}, \qquad \omega_k = \frac{\gamma_k}{(\beta_k + \varepsilon)^2}, \qquad k = 1,2,3, \tag{10}$$

where $\varepsilon$ is a small positive constant (typically $\varepsilon = 10^{-6}$), and

$$\gamma_1 = \frac{1}{16}, \qquad \gamma_2 = \frac{5}{8}, \qquad \gamma_3 = \frac{5}{16}. \tag{11}$$

The smoothness indicators are given by

$$\begin{aligned}
\beta_1 &= \frac{13}{12}(p_{j-2} - 2p_{j-1} + p_j)^2 + \frac{1}{4}(p_{j-2} - 4p_{j-1} + 3p_j)^2, \\
\beta_2 &= \frac{13}{12}(p_{j-1} - 2p_j + p_{j+1})^2 + \frac{1}{4}(p_{j-1} - p_{j+1})^2, \\
\beta_3 &= \frac{13}{12}(p_j - 2p_{j+1} + p_{j+2})^2 + \frac{1}{4}(3p_j - 4p_{j+1} + p_{j+2})^2.
\end{aligned} \tag{12}$$

The WENO methodology is designed to retain the full fifth-order accuracy in smooth regions while suppressing spurious oscillations near discontinuities. This is achieved by assigning smaller nonlinear weights to stencils that contain nonsmooth features, thereby favoring the smoother candidate reconstructions.

For convenience, we denote the reconstruction operator in (8) by

$$p^-_{j+\frac{1}{2}} = \mathrm{weno}(p_{j-2}, p_{j-1}, p_j, p_{j+1}, p_{j+2}).$$

The corresponding right limit value at $x_{j-\frac{1}{2}}$ is obtained by symmetry,

$$p^+_{j-\frac{1}{2}} = \mathrm{weno}(p_{j+2}, p_{j+1}, p_j, p_{j-1}, p_{j-2}).$$

This notation naturally extends to vector-valued quantities by applying the WENO reconstruction componentwise. For example,

$$\mathbf{p}^-_{j+\frac{1}{2}} = \mathrm{weno}(\mathbf{p}_{j-2}, \mathbf{p}_{j-1}, \mathbf{p}_j, \mathbf{p}_{j+1}, \mathbf{p}_{j+2}).$$

Finally, for any constant $c \in \mathbb{R}$,

$$\mathrm{weno}(c, c, c, c, c) = c,$$

which follows directly from the definition of the reconstruction.

### 2.2.2 The numerical flux

Suppose $\mathbf{h}(\cdot,\cdot)$ is a consistent numerical flux based on an exact or approximate Riemann solver, for instance, the Lax-Friedrichs flux $\mathbf{h}(\mathbf{w}^-, \mathbf{w}^+) = \frac{1}{2}\left(\mathbf{F}(\mathbf{w}^-) + \mathbf{F}(\mathbf{w}^+) - \alpha(\mathbf{w}^+ - \mathbf{w}^-)\right)$, where $\alpha$ is the maximum absolute value of the Jacobian of $\mathbf{F}(\mathbf{U})$. The high-order numerical flux $\hat{\mathbf{F}}$ in the A-WENO scheme is defined as follows:

$$\hat{\mathbf{F}}(\mathbf{U}_{j-2}, \cdots, \mathbf{U}_{j+3}) := \mathbf{h}(\mathbf{U}^-_{j+\frac{1}{2}}, \mathbf{U}^+_{j+\frac{1}{2}}) - \frac{1}{24}\Delta x^2 \left(\frac{\partial^2}{\partial x^2}\mathbf{F}\right)_{j+\frac{1}{2}} + \frac{7}{5760}\Delta x^4 \left(\frac{\partial^4}{\partial x^4}\mathbf{F}\right)_{j+\frac{1}{2}}, \tag{13}$$

where

$$\begin{aligned}
\left(\frac{\partial^2}{\partial x^2}\mathbf{F}\right)_{j+\frac{1}{2}} &= \frac{1}{\Delta x^2}\left(-\frac{5}{48}\mathbf{F}(\mathbf{U}_{j-2}) + \frac{13}{16}\mathbf{F}(\mathbf{U}_{j-1}) - \frac{17}{24}\mathbf{F}(\mathbf{U}_j) - \frac{17}{24}\mathbf{F}(\mathbf{U}_{j+1}) + \frac{13}{16}\mathbf{F}(\mathbf{U}_{j+2}) - \frac{5}{48}\mathbf{F}(\mathbf{U}_{j+3})\right), \\
\left(\frac{\partial^4}{\partial x^4}\mathbf{F}\right)_{j+\frac{1}{2}} &= \frac{1}{\Delta x^4}\left(\frac{1}{2}\mathbf{F}(\mathbf{U}_{j-2}) - \frac{3}{2}\mathbf{F}(\mathbf{U}_{j-1}) + \mathbf{F}(\mathbf{U}_j) + \mathbf{F}(\mathbf{U}_{j+1}) - \frac{3}{2}\mathbf{F}(\mathbf{U}_{j+2}) + \frac{1}{2}\mathbf{F}(\mathbf{U}_{j+3})\right).
\end{aligned}$$

are high-order central differences used to approximate $\frac{\partial^2}{\partial x^2}\mathbf{F}(\mathbf{U})$ and $\frac{\partial^4}{\partial x^4}\mathbf{F}(\mathbf{U})$ at $x_{j+\frac{1}{2}}$, respectively. What is crucial here is how we compute $\mathbf{U}^-_{j+\frac{1}{2}}$ and $\mathbf{U}^+_{j+\frac{1}{2}}$ that approximate the left and right limit value

of the solution at the interface $x_{j+\frac{1}{2}}$. In the ordinary (unbalanced) A-WENO scheme, $\mathbf{U}^-_{j+\frac{1}{2}}$ and $\mathbf{U}^+_{j+\frac{1}{2}}$ is taken to be the WENO interpolation along the local characteristic field [7]:

$$\begin{aligned}\mathbf{U}^-_{j+\frac{1}{2}} &= \mathbf{R}_{j+\frac{1}{2}}\,\mathrm{weno}(\mathbf{R}^{-1}_{j+\frac{1}{2}}\,\mathbf{U}_{j-2},\cdots,\mathbf{R}^{-1}_{j+\frac{1}{2}}\,\mathbf{U}_{j+2}),\\ \mathbf{U}^+_{j+\frac{1}{2}} &= \mathbf{R}_{j+\frac{1}{2}}\,\mathrm{weno}(\mathbf{R}^{-1}_{j+\frac{1}{2}}\,\mathbf{U}_{j+3},\cdots,\mathbf{R}^{-1}_{j+\frac{1}{2}}\,\mathbf{U}_{j-1}),\end{aligned}$$

where $\mathbf{R}_{j+\frac{1}{2}}$ is the matrix of right eigenvectors of the Jacobian matrix $\frac{\partial \mathbf{F}}{\partial \mathbf{U}}(\mathbf{U}_{j+\frac{1}{2}})$, and the value $\mathbf{U}_{j+\frac{1}{2}}$ is obtained by either the arithmetic mean or Roe's average [17] of $\mathbf{U}_j$ and $\mathbf{U}_{j+1}$. However, if we interpolate this way, the scheme (7) with $\hat{\mathbf{F}}$ defined as above would not be conservative for those equations with the source term being identically zero. To overcome this difficulty, we first transform $\mathbf{U}_k$ to $\mathbf{V}_k := \mathbf{V}(\mathbf{U}_k, x_k)$ for all $k$, then perform the WENO interpolation on $\mathbf{V}_k$'s instead to obtain $\mathbf{V}^\pm_{j+\frac{1}{2}}$, and finally transform it back to $\mathbf{U}^\pm_{j+\frac{1}{2}} = \mathbf{U}(\mathbf{V}^\pm_{j+\frac{1}{2}}, x_{j+\frac{1}{2}})$; namely, we set

$$\begin{aligned}\mathbf{U}^-_{j+\frac{1}{2}} &= \mathbf{U}\left(\mathbf{K}_{j+\frac{1}{2}}\,\mathrm{weno}\left(\mathbf{K}^{-1}_{j+\frac{1}{2}}\,\mathbf{V}(\mathbf{U}_{j-2},x_{j-2}),\cdots,\mathbf{K}^{-1}_{j+\frac{1}{2}}\,\mathbf{V}(\mathbf{U}_{j+2},x_{j+2})\right),x_{j+\frac{1}{2}}\right),\\ \mathbf{U}^+_{j+\frac{1}{2}} &= \mathbf{U}\left(\mathbf{K}_{j+\frac{1}{2}}\,\mathrm{weno}\left(\mathbf{K}^{-1}_{j+\frac{1}{2}}\,\mathbf{V}(\mathbf{U}_{j+3},x_{j+3}),\cdots,\mathbf{K}^{-1}_{j+\frac{1}{2}}\,\mathbf{V}(\mathbf{U}_{j-1},x_{j-1})\right),x_{j+\frac{1}{2}}\right),\end{aligned}$$

where $\mathbf{K}_{j+\frac{1}{2}} = \frac{\partial \mathbf{V}}{\partial \mathbf{U}}(\mathbf{U}_{j+\frac{1}{2}}, x_{j+\frac{1}{2}})\mathbf{R}_{j+\frac{1}{2}}$, with $\mathbf{R}_{j+\frac{1}{2}}$ and $\mathbf{U}_{j+\frac{1}{2}}$ being defined as before. With this modified WENO interpolation on the equilibrium variables, the scheme has become conservative. To see this, recall that any set of equilibrium variables $\mathbf{V}(\mathbf{U}(x),x)$ is constant throughout the physical space when $\mathbf{U}$ is in an equilibrium state. If the source term is identically zero in the $i$th equation of the system of balance laws (5) (in which case it becomes a conservation law), namely, $s_i(x,\mathbf{U}) \equiv 0$ and $(u_i)_t + f_i(\mathbf{U})_x = 0$, and the corresponding equation in the numerical scheme (7) becomes

$$\begin{aligned}&\frac{\mathrm{d}(u_i)_j}{\mathrm{d}t} + \frac{1}{\Delta x}\left(\hat{f}_i(\mathbf{U}_{j-2},\cdots,\mathbf{U}_{j+3}) - \hat{f}_i(\mathbf{U}_{j-3},\cdots,\mathbf{U}_{j+2})\right)\\ =&\frac{1}{\Delta x}\left(\hat{f}_i(\mathbf{U}_{e,j}(x_{j-2}),\cdots,\mathbf{U}_{e,j}(x_{j+3})) - \hat{f}_i(\mathbf{U}_{e,j}(x_{j-3}),\cdots,\mathbf{U}_{e,j}(x_{j+2}))\right).\end{aligned} \tag{14}$$

We now show that the right-hand side of (14) vanishes, so that this scheme is indeed conservative. At any equilibrium state $\mathbf{U}_e(x)$, $f_i(\mathbf{U}_e)$ would be constant throughout the physical domain (since $s_i(x,\mathbf{U}) \equiv 0$). In particular, this holds for the specially constructed equilibrium state $\mathbf{U}_{e,j}(x)$, so that if we replace $\mathbf{U}_k$ by $\mathbf{U}_{e,j}(x_k)$ in the definition of the numerical flux (13), the last two terms in its $i$th component would become zero. Furthermore, since $\mathbf{V}(\mathbf{U}_{e,j}(x),x)$ is constant (say equals to $\mathbf{V}_e$) for all $x \in \mathbb{R}$ and $\mathrm{weno}(c,c,c,c,c) = c$, we have

$$\begin{aligned}\mathbf{U}^-_{j+\frac{1}{2}} =&\mathbf{U}\left(\mathbf{K}_{j+\frac{1}{2}}\,\mathrm{weno}\left(\mathbf{K}^{-1}_{j+\frac{1}{2}}\,\mathbf{V}(\mathbf{U}_{e,j}(x_{j-2}),x_{j-2}),\cdots,\mathbf{K}^{-1}_{j+\frac{1}{2}}\,\mathbf{V}(\mathbf{U}_{e,j}(x_{j+2}),x_{j+2})\right),x_{j+\frac{1}{2}}\right),\\ =&\mathbf{U}\left(\mathbf{K}_{j+\frac{1}{2}}\,\mathrm{weno}\left(\mathbf{K}^{-1}_{j+\frac{1}{2}}\,\mathbf{V}_e,\cdots,\mathbf{K}^{-1}_{j+\frac{1}{2}}\,\mathbf{V}_e\right),x_{j+\frac{1}{2}}\right),\\ =&\mathbf{U}\left(\mathbf{V}_e,x_{j+\frac{1}{2}}\right)\\ =&\mathbf{U}_{e,j}(x_{j+\frac{1}{2}})\\ =&\mathbf{U}\left(\mathbf{K}_{j+\frac{1}{2}}\,\mathrm{weno}\left(\mathbf{K}^{-1}_{j+\frac{1}{2}}\,\mathbf{V}_e,\cdots,\mathbf{K}^{-1}_{j+\frac{1}{2}}\,\mathbf{V}_e\right),x_{j+\frac{1}{2}}\right),\\ =&\mathbf{U}\left(\mathbf{K}_{j+\frac{1}{2}}\,\mathrm{weno}\left(\mathbf{K}^{-1}_{j+\frac{1}{2}}\,\mathbf{V}(\mathbf{U}_{e,j}(x_{j+3}),x_{j+3}),\cdots,\mathbf{K}^{-1}_{j+\frac{1}{2}}\,\mathbf{V}(\mathbf{U}_{e,j}(x_{j-1}),x_{j-1})\right),x_{j+\frac{1}{2}}\right)\\ =&\mathbf{U}^+_{j+\frac{1}{2}}.\end{aligned}$$

Thus, the first term in the $i$th component of (13) becomes $f_i(\mathbf{U}_{e,j}(x_{j+\frac{1}{2}}))$, which gives

$$\hat{f}_i(\mathbf{U}_{e,j}(x_{j-2}),\cdots,\mathbf{U}_{e,j}(x_{j+3})) = f_i(\mathbf{U}_{e,j}(x_{j+\frac{1}{2}})).$$

In the same way, we also find that

$$\hat{f}_i(\mathbf{U}_{e,j}(x_{j-3}),\cdots,\mathbf{U}_{e,j}(x_{j+2})) = f_i(\mathbf{U}_{e,j}(x_{j+\frac{1}{2}})),$$

so that the right-hand side of (14) indeed vanishes and the scheme is conservative. Moreover, one does not actually need to compute the WENO interpolation in $\hat{\mathbf{F}}$ on the right-hand side of the scheme (7). Since $\mathbf{V}(\mathbf{U}_{e,j}(x),x)$ is constant and $\mathrm{weno}(c,c,c,c,c) = c$, we have

$$\mathbf{U}^-_{j+\frac{1}{2}} = \mathbf{U}^+_{j+\frac{1}{2}} = \mathbf{U}_{e,j}(x_{j+\frac{1}{2}}),$$

which minimizes the computational costs in approximating the source term.

Note that at this point, we still have not explained how to construct the local equilibrium state $\mathbf{U}_{e,j}(x)$ based on the point values $\{\mathbf{U}_{j-3},\cdots,\mathbf{U}_{j+3}\}$. This will be the task of Section 2.4.

## 2.3 Extension to multidimensional systems

Consider a generic system of hyperbolic balance laws in $n$ space dimensions defined in $\mathbb{R}^n$ where the source term $\mathbf{S}(x_1,\mathbf{U})$ only depends on one coordinate $x_1$:

$$\frac{\partial \mathbf{U}}{\partial t} + \sum_{i=1}^{n} \frac{\partial \mathbf{F}^{(i)}(\mathbf{U})}{\partial x_i} = \mathbf{S}(x_1,\mathbf{U}), \quad \mathbf{x} = (x_1,x_2,\cdots,x_n) \in \mathbb{R}^n. \tag{15}$$

Suppose $\mathbf{U}, \mathbf{F}^{(1)}(\mathbf{U}),\cdots,\mathbf{F}^{(n)}(\mathbf{U}), \mathbf{S}(x_1,\mathbf{U}) \in \mathbb{R}^N$. As in the one dimensional case, we assume that there exists a transformation $\mathbf{V} = \mathbf{V}(\mathbf{U},\mathbf{x}) \in \mathbb{R}^N$ such that $\mathbf{V}(\mathbf{U},\mathbf{x})$ is constant throughout the physical space when $\mathbf{U}$ is in an equilibrium state ($\mathbf{V}$ is called the vector of equilibrium variables). In this paper, we only aim to preserve those equilibrium states that depend only on the first coordinate $x_1$, in which case we may find a transformation $\mathbf{V}(\mathbf{U},\mathbf{x}) = \mathbf{V}(\mathbf{U},x_1)$ that depends only on $x_1$ as well. For now, we assume that the transformation $\mathbf{U} \to \mathbf{V}(\mathbf{U},x_1)$ is invertible (again, this is technically not true for the equilibrium variables adopted in this paper; we will see how to resolve this issue in Section 2.4) and denote its inverse by $\mathbf{U} = \mathbf{U}(\mathbf{V},x_1)$. Let the $n$-dimensional space be discretized by a rectangular grid with uniform mesh size $\Delta x_i$ on each coordinate $x_i$, $i = 1,\cdots,n$. Set $\mathbf{j} := (j_1,j_2,\cdots,j_n)$ where $j_i \in \mathbb{Z}$ for all $i = 1,2,\cdots,n$. The numerical solution is defined at the vertices of the rectangular grid, that is, at the points

$$\mathbf{x}_\mathbf{j} := (j_1\Delta x_1, j_2\Delta x_2,\cdots,j_n\Delta x_n),$$

where $j_i \in \mathbb{Z}$ for all $i = 1,2,\cdots,n$. Denote the $i$th coordinate of $\mathbf{x}_\mathbf{j}$ by $\mathbf{x}_\mathbf{j}(i) := j_i\Delta x_i$. The value of the numerical solution at the point $\mathbf{x}_\mathbf{j}$ is denoted by $\mathbf{U}(\mathbf{j})$. We also let

$$\mathbf{e}_1 = (1,0,\cdots,0), \mathbf{e}_2 = (0,1,\cdots,0),\cdots,\mathbf{e}_n = (0,0,\cdots,1),$$

that is, the vector $\mathbf{e}_i$ has 1 in its $i$-th entry and 0 in the other positions. The well-balanced fifth-order A-WENO scheme in $n$ space dimensions can then be written as

$$\begin{aligned}
&\frac{\mathrm{d}\mathbf{U}(\mathbf{j})}{\mathrm{d}t} + \sum_{i=1}^{n} \frac{1}{\Delta x_i}\left(\hat{\mathbf{F}}^{(i)}(\mathbf{U}(\mathbf{j}-2\mathbf{e}_i),\cdots,\mathbf{U}(\mathbf{j}+3\mathbf{e}_i)) - \hat{\mathbf{F}}^{(i)}(\mathbf{U}(\mathbf{j}-3\mathbf{e}_i),\cdots,\mathbf{U}(\mathbf{j}+2\mathbf{e}_i))\right)\\
=&\frac{\mathbf{S}(\mathbf{x}_\mathbf{j}(1),\mathbf{U}(\mathbf{j}))}{\mathbf{S}(\mathbf{x}_\mathbf{j}(1),\mathbf{U}_{e,\mathbf{j}}(\mathbf{j}))} \sum_{i=1}^{n} \frac{1}{\Delta x_i}\left(\hat{\mathbf{F}}^{(i)}(\mathbf{U}_{e,\mathbf{j}}(\mathbf{j}-2\mathbf{e}_i),\cdots,\mathbf{U}_{e,\mathbf{j}}(\mathbf{j}+3\mathbf{e}_i)) - \hat{\mathbf{F}}^{(i)}(\mathbf{U}_{e,\mathbf{j}}(\mathbf{j}-3\mathbf{e}_i),\cdots,\mathbf{U}_{e,\mathbf{j}}(\mathbf{j}+2\mathbf{e}_i))\right),
\end{aligned} \tag{16}$$

where again, the operations on the right-hand side are to be understood as component-wise. $\mathbf{U}_{e,\mathbf{j}}$ denotes the special equilibrium state constructed locally from the information near the vertex $\mathbf{x}_\mathbf{j}$, and $\mathbf{U}_{e,\mathbf{j}}(\mathbf{k})$ denotes the value of $\mathbf{U}_{e,\mathbf{j}}$ evaluated at $\mathbf{x}_\mathbf{k}$. Since the source term $\mathbf{S}(x_1,\mathbf{U})$ depends only on

the first coordinate $x_1$, we can construct $\mathbf{U}_{e,\mathbf{j}}(\mathbf{x}) = \mathbf{U}_{e,\mathbf{j}}(x_1)$ as a function that depends only on $x_1$ as well. In Section 2.4, we will show how to construct such a $\mathbf{U}_{e,\mathbf{j}}(x_1)$ based on the point values $\{\mathbf{U}(\mathbf{j}-3\mathbf{e}_1),\cdots,\mathbf{U}(\mathbf{j}+3\mathbf{e}_1)\}$. Exactly parallel to the one dimensional case, $\hat{\mathbf{F}}^{(i)}(\mathbf{U}(\mathbf{j}-2\mathbf{e}_i),\cdots,\mathbf{U}(\mathbf{j}+3\mathbf{e}_i))$ is defined as

$$\begin{aligned}\hat{\mathbf{F}}^{(i)}(\mathbf{U}(\mathbf{j}-2\mathbf{e}_i),\cdots,\mathbf{U}(\mathbf{j}+3\mathbf{e}_i)) :=& \mathbf{h}^{(i)}\left(\mathbf{U}^-\left(\mathbf{j}+\frac{1}{2}\mathbf{e}_i\right),\mathbf{U}^+\left(\mathbf{j}+\frac{1}{2}\mathbf{e}_i\right)\right)\\ &-\frac{1}{24}\Delta x_i^2\left(\frac{\partial^2}{\partial x_i^2}\mathbf{F}^{(i)}\right)\left(\mathbf{j}+\frac{1}{2}\mathbf{e}_i\right)\\ &+\frac{7}{5760}\Delta x_i^4\left(\frac{\partial^4}{\partial x_i^4}\mathbf{F}^{(i)}\right)\left(\mathbf{j}+\frac{1}{2}\mathbf{e}_i\right).\end{aligned}$$

In the last expression, $\mathbf{h}^{(i)}(\cdot,\cdot)$ is taken to be the Lax–Friedrichs flux consistent with $\mathbf{F}^{(i)}(\mathbf{U})$, that is, $\mathbf{h}^{(i)}(\mathbf{U}^-,\mathbf{U}^+) = \frac{1}{2}(\mathbf{F}^{(i)}(\mathbf{U}^-)+\mathbf{F}^{(i)}(\mathbf{U}^+)-\alpha(\mathbf{U}^+-\mathbf{U}^-))$, with $\alpha$ representing the maximum absolute value of the eigenvalues of the Jacobian of $\mathbf{F}^{(i)}(\mathbf{U})$, and

$$\begin{aligned}\left(\frac{\partial^2}{\partial x_i^2}\mathbf{F}^{(i)}\right)\left(\mathbf{j}+\frac{1}{2}\mathbf{e}_i\right) :=& \frac{1}{\Delta x_i^2}\left(-\frac{5}{48}\mathbf{F}^{(i)}(\mathbf{U}(\mathbf{j}-2\mathbf{e}_i))+\frac{13}{16}\mathbf{F}^{(i)}(\mathbf{U}(\mathbf{j}-\mathbf{e}_i))-\frac{17}{24}\mathbf{F}^{(i)}(\mathbf{U}(\mathbf{j}))\right.\\ &\left.-\frac{17}{24}\mathbf{F}^{(i)}(\mathbf{U}(\mathbf{j}+\mathbf{e}_i))+\frac{13}{16}\mathbf{F}^{(i)}(\mathbf{U}(\mathbf{j}+2\mathbf{e}_i))-\frac{5}{48}\mathbf{F}^{(i)}(\mathbf{U}(\mathbf{j}+3\mathbf{e}_i))\right),\\ \left(\frac{\partial^4}{\partial x_i^4}\mathbf{F}^{(i)}\right)\left(\mathbf{j}+\frac{1}{2}\mathbf{e}_i\right) :=& \frac{1}{\Delta x_i^4}\left(\frac{1}{2}\mathbf{F}^{(i)}(\mathbf{U}(\mathbf{j}-2\mathbf{e}_i))-\frac{3}{2}\mathbf{F}^{(i)}(\mathbf{U}(\mathbf{j}-\mathbf{e}_i))+\mathbf{F}^{(i)}(\mathbf{U}(\mathbf{j}))\right.\\ &\left.+\mathbf{F}^{(i)}(\mathbf{U}(\mathbf{j}+\mathbf{e}_i))-\frac{3}{2}\mathbf{F}^{(i)}(\mathbf{U}(\mathbf{j}+2\mathbf{e}_i))+\frac{1}{2}\mathbf{F}^{(i)}(\mathbf{U}(\mathbf{j}+3\mathbf{e}_i))\right)\end{aligned}$$

are higher-order central differences approximating $\frac{\partial^2}{\partial x_i^2}\mathbf{F}^{(i)}(\mathbf{U})$ and $\frac{\partial^4}{\partial x_i^4}\mathbf{F}^{(i)}(\mathbf{U})$ respectively at the point

$$\left(j_1\Delta x_1,\cdots,\left(j_i+\frac{1}{2}\right)\Delta x_i,\cdots,j_n\Delta x_n\right).$$

When interpolating the values at the interfaces using WENO, only the component in the first coordinate needs the transformation to the equilibrium variables:

$$\begin{aligned}\mathbf{U}^-\left(\mathbf{j}+\frac{1}{2}\mathbf{e}_1\right) &= \mathbf{U}\left(\mathbf{K}_{j+\frac{1}{2}}\,\mathrm{weno}\left(\mathbf{K}^{-1}_{j+\frac{1}{2}}\mathbf{V}(\mathbf{U}(\mathbf{j}-2\mathbf{e}_1),\mathbf{x}_{\mathbf{j}-2\mathbf{e}_1}),\cdots,\mathbf{K}^{-1}_{j+\frac{1}{2}}\mathbf{V}(\mathbf{U}(\mathbf{j}+2\mathbf{e}_1),\mathbf{x}_{\mathbf{j}+2\mathbf{e}_1})\right),\mathbf{x}_{\mathbf{j}+\frac{1}{2}}\right),\\ \mathbf{U}^+\left(\mathbf{j}+\frac{1}{2}\mathbf{e}_1\right) &= \mathbf{U}\left(\mathbf{K}_{j+\frac{1}{2}}\,\mathrm{weno}\left(\mathbf{K}^{-1}_{j+\frac{1}{2}}\mathbf{V}(\mathbf{U}(\mathbf{j}+3\mathbf{e}_1),\mathbf{x}_{\mathbf{j}+3\mathbf{e}_1}),\cdots,\mathbf{K}^{-1}_{j+\frac{1}{2}}\mathbf{V}(\mathbf{U}(\mathbf{j}-\mathbf{e}_1),\mathbf{x}_{\mathbf{j}-\mathbf{e}_1})\right),\mathbf{x}_{\mathbf{j}+\frac{1}{2}}\right),\end{aligned}$$

while others are interpolated without the transformation:

$$\begin{aligned}\mathbf{U}^-\left(\mathbf{j}+\frac{1}{2}\mathbf{e}_i\right) &= \mathrm{weno}(\mathbf{U}(\mathbf{j}-2\mathbf{e}_i),\cdots,\mathbf{U}(\mathbf{j}+2\mathbf{e}_i)),\quad i=2,\cdots,n,\\ \mathbf{U}^+\left(\mathbf{j}+\frac{1}{2}\mathbf{e}_i\right) &= \mathrm{weno}(\mathbf{U}(\mathbf{j}+3\mathbf{e}_i),\cdots,\mathbf{U}(\mathbf{j}-\mathbf{e}_i)),\quad i=2,\cdots,n.\end{aligned}$$

In Section 2.4, we will show explicitly how to construct the local equilibrium state $\mathbf{U}_{e,\mathbf{j}}(\mathbf{x}) = \mathbf{U}_{e,\mathbf{j}}(x_1)$ based on the point values $\{\mathbf{U}(\mathbf{j}-3\mathbf{e}_1),\cdots,\mathbf{U}(\mathbf{j}+3\mathbf{e}_1)\}$.

## 2.4 Equilibrium variables for Euler equations

In this section we provide the explicit expressions for the equilibrium variables $\mathbf{V}(\mathbf{U},x_1)$ for Euler equations in 2D and 3D, and show how to construct the local equilibrium state $\mathbf{U}_{e,\mathbf{j}}(x_1)$ from the point values $\{\mathbf{U}(\mathbf{j}-3\mathbf{e}_1),\cdots,\mathbf{U}(\mathbf{j}+3\mathbf{e}_1)\}$. As mentioned previously, the transformation $\mathbf{U}\to\mathbf{V}(\mathbf{U},x_1)$ for Euler equations is technically not invertible; in particular, for each $\mathbf{V}_0$, there generally exist two different $\mathbf{U}$'s, one corresponds to the supersonic flow ($\text{Mach}(\mathbf{U})>1$) and the other corresponds to the subsonic flow ($\text{Mach}(\mathbf{U})<1$), such that they both satisfy $\mathbf{V}_0=\mathbf{V}(\mathbf{U},x_1)$; only in the case when $\text{Mach}(\mathbf{U})=1$ does the two solutions coincide. Recall that the inverse transform is only used when converting the WENO interpolation along the first coordinate of $\mathbf{V}$ back to $\mathbf{U}$. In what follows, we will see how to resolve this issue by choosing the correct Mach number based on the values of $\mathbf{U}$ near the interface.

### 2.4.1 2D Euler equations in Cartesian coordinates

The 2D Cartesian coordinate variables are denoted by $(x,y)$. The 2D Euler equations with gravity potential $\Phi(x,y)$ in conservative form and Cartesian coordinates can be written as follows:

$$\frac{\partial\mathbf{U}}{\partial t}+\frac{\partial\mathbf{F}(\mathbf{U})}{\partial x}+\frac{\partial\mathbf{G}(\mathbf{U})}{\partial y}=\mathbf{S}(x,y,\mathbf{U}), \tag{17}$$

where $\mathbf{U}=(\rho,\rho u,\rho v,E)^T=(\rho,m,n,E)^T$ is the vector of conservative variables, and

$$\mathbf{F}(\mathbf{U})=(\rho u,\rho u^2+p,\rho uv,u(E+p))^T=(m,m^2/\rho+p,mn/\rho,m(E+p)/\rho)^T, \tag{18}$$

$$\mathbf{G}(\mathbf{U})=(\rho v,\rho uv,\rho v^2+p,v(E+p))^T=(n,mn/\rho,n^2/\rho+p,n(E+p)/\rho)^T, \tag{19}$$

$$\mathbf{S}(x,y,\mathbf{U})=(0,-\rho\Phi_x,-\rho\Phi_y,-m\Phi_x-n\Phi_y)^T. \tag{20}$$

In the above, $u$ and $v$ denote respectively the velocity in the $x$- and $y$-direction; $m:=\rho u$ and $n:=\rho v$ denote respectively the momentum in the $x$- and $y$-direction. *In this paper, we only consider the situation where the potential $\Phi(x,y)=\Phi(x)$ is independent of $y$ and monotone in $x$, and we only attempt to preserve isentropic steady states that depend only on $x$, i.e. with $n=0$.* Since $\Phi$ only depends on $x$, we have $\mathbf{S}(x,y,\mathbf{U})=\mathbf{S}(x,\mathbf{U})$. The scheme is defined as in equation (16) from the previous section by setting $n=2$, $x_1=x$ and $x_2=y$, together with the mesh size $\Delta x_1=\Delta x$ and $\Delta x_2=\Delta y$. At a given node $\mathbf{x}_\mathbf{j}=(x_{j_1},y_{j_2})=(j_1\Delta x,j_2\Delta y)$, the fourth component of the denominator in the quotient $\frac{\mathbf{S}(\mathbf{x}_\mathbf{j}(1),\mathbf{U}(\mathbf{j}))}{\mathbf{S}(\mathbf{x}_\mathbf{j}(1),\mathbf{U}_{e,\mathbf{j}}(\mathbf{j}))}$ from (16), namely $-m_{e,\mathbf{j}}\Phi_x(x_{j_1})$, might turn zero if $m_{e,\mathbf{j}}=0$, but since $m_{e,\mathbf{j}}$ is constant for the local equilibrium state $\mathbf{U}_{e,\mathbf{j}}$, it can be canceled by the same factor in the flux difference, so no zero divisor will occur. For isentropic steady states, the following two quantities are constant along streamlines:

$$s=\frac{p}{\rho^\gamma},\quad Q=\frac{m^2+n^2}{2\rho^2}+\frac{\gamma s\rho^{\gamma-1}}{\gamma-1}+\Phi(x).$$

Since the equilibrium states considered in this paper only depend on $x$ with $n=0$, the above two expressions are constant over the entire domain of computation. In addition, for such steady states we also have

$$m=\text{constant},\quad n=0=\text{constant}.$$

Thus, the transformation to the equilibrium variables is defined as follows:

$$\begin{aligned}\mathbf{V}(\mathbf{U},x)=\mathbf{V}(\rho,m,n,E,x):=(s,m,n,Q)^T&=\left(\frac{p}{\rho^\gamma},m,n,\frac{m^2+n^2}{2\rho^2}+\frac{\gamma s\rho^{\gamma-1}}{\gamma-1}+\Phi(x)\right)^T\\&=\left(\frac{\gamma-1}{\rho^\gamma}\left(E-\frac{m^2+n^2}{2\rho}\right),m,n,(1-\gamma)\frac{m^2+n^2}{2\rho^2}+\frac{\gamma E}{\rho}+\Phi(x)\right)^T.\end{aligned}$$

When we perform the inverse transform $\mathbf{U} = \mathbf{U}(\mathbf{V}, x)$, the value of $(s, m, n, Q)$ is known, so we can first determine $\rho$ by solving the following nonlinear equation:

$$\frac{m^2+n^2}{2\rho^2} + \frac{\gamma s \rho^{\gamma-1}}{\gamma-1} + \Phi(x) = Q. \tag{21}$$

Then, with this $\rho$ just obtained, $E$ can be computed from

$$E = \frac{m^2+n^2}{2\rho} + \frac{\rho^\gamma s}{\gamma-1}.$$

However, note that unless $\text{Mach}(\mathbf{U}) = 1$, the nonlinear equation (21) for $\rho$ generally has two different solutions. Indeed, let

$$\psi(\rho) := \frac{m^2+n^2}{2\rho^2} + \frac{\gamma s \rho^{\gamma-1}}{\gamma-1}.$$

Then, the nonlinear equation (21) is equivalent to $\psi(\rho) = Q - \Phi(x)$. The function $\psi$ has two branches, one decreasing and one increasing, see Figure 1.

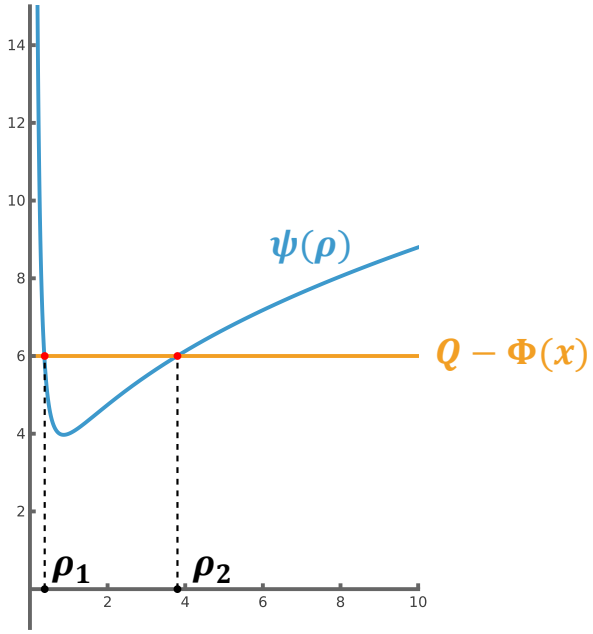



Figure 1: The graph of $\psi(\rho)$ when $m^2+n^2 = s = 1$ and $\gamma = 1.4$. In the above, $Q - \Phi(x) = 6$, which is greater than the minimum value of $\psi(\rho)$. Thus, there are two roots $\rho_1$ and $\rho_2$, the former corresponds to Mach $> 1$ and the latter Mach $< 1$.

The local minimum of $\psi(\rho)$ is found to be

$$\psi(\rho) = \frac{m^2+n^2}{2\rho^2} + \frac{\gamma s \rho^{\gamma-1}}{\gamma-1} \geq \frac{\gamma+1}{2(\gamma-1)} (\gamma s)^{\frac{2}{\gamma+1}} (m^2+n^2)^{\frac{\gamma-1}{\gamma+1}},$$

where equality holds if and only if $\rho^{\gamma+1} = \frac{m^2+n^2}{\gamma s}$, that is, $\text{Mach}(\mathbf{U}) = \sqrt{\frac{m^2+n^2}{\gamma s \rho^{\gamma+1}}} = 1$. If $Q - \Phi(x) < \frac{\gamma+1}{2(\gamma-1)} (\gamma s)^{\frac{2}{\gamma+1}} (m^2+n^2)^{\frac{\gamma-1}{\gamma+1}}$, equation (21) has no solution; if $Q - \Phi(x) = \frac{\gamma+1}{2(\gamma-1)} (\gamma s)^{\frac{2}{\gamma+1}} (m^2+n^2)^{\frac{\gamma-1}{\gamma+1}}$, there is a unique solution with Mach $= 1$; if $Q - \Phi(x) > \frac{\gamma+1}{2(\gamma-1)} (\gamma s)^{\frac{2}{\gamma+1}} (m^2+n^2)^{\frac{\gamma-1}{\gamma+1}}$, there are two solutions, the smaller one corresponds to Mach $> 1$ (supersonic), and the larger one corresponds to Mach $< 1$ (subsonic).

Therefore, the inverse transform from $\mathbf{V}$ to $\mathbf{U}$ also has two different values in general, in which case the sign of $\mathrm{Mach}(\mathbf{U})-1$ is needed for determining which value to choose. When computing $\mathbf{U}^-\left(\mathbf{j}+\frac{1}{2}\mathbf{e}_1\right)$ and $\mathbf{U}^+\left(\mathbf{j}+\frac{1}{2}\mathbf{e}_1\right)$ for the numerical flux on the left-hand side of (16), we take the Mach number of $\mathbf{U}(\mathbf{j})$ and $\mathbf{U}(\mathbf{j}+\mathbf{e}_1)$ respectively for the inverse transform (note that the inverse transform is only required for the first coordinate $x_1 = x$).

For any fixed $\mathbf{j} = (j_1, j_2)$, we construct the local equilibrium state $\mathbf{U}_{e,\mathbf{j}}(x)$ based on the point values $\{\mathbf{U}(\mathbf{j}-3\mathbf{e}_1), \cdots, \mathbf{U}(\mathbf{j}+3\mathbf{e}_1)\}$ as follows:

$$\mathbf{U}_{e,\mathbf{j}}(x) = \mathbf{U}(\mathbf{V}(\rho(\mathbf{j}+\beta\,\mathbf{e}_1), m(\mathbf{j}+\beta\,\mathbf{e}_1), 0, E(\mathbf{j}+\beta\,\mathbf{e}_1), x_{j_1+\beta}), x),$$

where $\beta \in \{-3, 3\}$ is the index such that $\Phi((j_1+\beta)\Delta x)$ obtains its maximum on the interval $[(j_1-3)\Delta x, (j_1+3)\Delta x]$ (recall that $\Phi(x)$ is monotone, so its maximum is attained at one of the end points of the interval). More precisely, let $(s_{e,\mathbf{j}}, m_{e,\mathbf{j}}, 0, Q_{e,\mathbf{j}}) := \mathbf{V}(\rho(\mathbf{j}+\beta\,\mathbf{e}_1), m(\mathbf{j}+\beta\,\mathbf{e}_1), 0, E(\mathbf{j}+\beta\,\mathbf{e}_1), x_{j_1+\beta})$; then, in order to compute the local equilibrium state $\mathbf{U}_{e,\mathbf{j}}(x)$ for any $x$, we need to first solve the following equation for $\rho(x)$:

$$Q_{e,\mathbf{j}} - \Phi(x) = \frac{m_{e,\mathbf{j}}^2}{2\rho(x)^2} + \frac{\gamma \cdot s_{e,\mathbf{j}} \cdot \rho(x)^{\gamma-1}}{\gamma-1}, \tag{22}$$

and finally compute $E(x)$ from

$$E(x) = \frac{m_{e,\mathbf{j}}^2}{2\rho(x)} + \frac{\rho(x)^\gamma}{\gamma-1} s_{e,\mathbf{j}}.$$

With this choice, one can guarantee that $\mathbf{U}_{e,\mathbf{j}}(x)$ is well-defined on the interval $[(j_1-3)\Delta x, (j_1+3)\Delta x]$, since for all $x \in [(j_1-3)\Delta x, (j_1+3)\Delta x]$ we have

$$Q_{e,\mathbf{j}} - \Phi(x) \geq Q_{e,\mathbf{j}} - \Phi(x_{j_1+\beta}) \geq \frac{\gamma+1}{2(\gamma-1)} (\gamma s_{e,\mathbf{j}})^{\frac{2}{\gamma+1}} (m_{e,\mathbf{j}}^2)^{\frac{\gamma-1}{\gamma+1}},$$

so that equation (22) is always solvable. However, we would still need to resolve the issue that the solution to the above equation is not unique. To this end, when performing the inverse transform, we set the sign of $\mathrm{Mach}-1$ to be the same as that of $\mathbf{U}(\mathbf{j}+\beta\,\mathbf{e}_1)$. Since $\Phi(x)$ is monotone, the sign of $\mathrm{Mach}-1$ does not change for any essentially 1D isentropic steady state of Euler equations (see Section 2.5), so that the resulting scheme is still well-balanced.

### 2.4.2 3D Euler equations in Cartesian coordinates

The 3D Cartesian coordinate variables are denoted by $(x, y, z)$. The 3D Euler equations with gravity potential $\Phi(x, y, z)$ in conservative form and Cartesian coordinates can be written as follows:

$$\frac{\partial \mathbf{U}}{\partial t} + \frac{\partial \mathbf{F}(\mathbf{U})}{\partial x} + \frac{\partial \mathbf{G}(\mathbf{U})}{\partial y} + \frac{\partial \mathbf{H}(\mathbf{U})}{\partial z} = \mathbf{S}(x, y, z, \mathbf{U}), \tag{23}$$

where $\mathbf{U} = (\rho, \rho u, \rho v, \rho w, E)^T = (\rho, m, n, l, E)^T$ is the vector of conservative variables, and

$$\mathbf{F}(\mathbf{U}) = (\rho u, \rho u^2 + p, \rho uv, \rho uw, u(E+p))^T = (m, m^2/\rho + p, mn/\rho, ml/\rho, m(E+p)/\rho)^T, \tag{24}$$

$$\mathbf{G}(\mathbf{U}) = (\rho v, \rho uv, \rho v^2 + p, \rho vw, v(E+p))^T = (n, mn/\rho, n^2/\rho + p, nl/\rho, n(E+p)/\rho)^T, \tag{25}$$

$$\mathbf{H}(\mathbf{U}) = (\rho w, \rho uw, \rho vw, \rho w^2 + p, w(E+p))^T = (l, ml/\rho, nl/\rho, l^2/\rho + p, l(E+p)/\rho)^T, \tag{26}$$

$$\mathbf{S}(x, y, z, \mathbf{U}) = (0, -\rho\Phi_x, -\rho\Phi_y, -\rho\Phi_z, -m\Phi_x - n\Phi_y - l\Phi_z)^T. \tag{27}$$

In the above, $u$, $v$ and $w$ denote respectively the velocity in the $x$-, $y$- and $z$-direction; $m := \rho u$, $n := \rho v$ and $l := \rho w$ denote respectively the momentum in the $x$-, $y$- and $z$-direction. *In this paper, we only consider the situation where the potential $\Phi(x, y, z) = \Phi(x)$ is independent of $y, z$ and monotone in $x$,*

*and we only attempt to preserve isentropic steady states that depend only on x, i.e. with* $n = l = 0$. Under this assumption, $\mathbf{S}(x, y, z, \mathbf{U}) = \mathbf{S}(x, \mathbf{U})$. The scheme is defined as in equation (16) by setting $n = 3$, $x_1 = x$, $x_2 = y$ and $x_3 = z$, together with the mesh size $\Delta x_1 = \Delta x$, $\Delta x_2 = \Delta y$ and $\Delta x_3 = \Delta z$. At a given node $\mathbf{x_j} = (x_{j_1}, y_{j_2}, z_{j_3}) = (j_1\Delta x, j_2\Delta y, j_3\Delta z)$, the fifth component of the denominator in the quotient $\frac{\mathbf{S}(\mathbf{x_j}(1), \mathbf{U}(\mathbf{j}))}{\mathbf{S}(\mathbf{x_j}(1), \mathbf{U}_{e,\mathbf{j}}(\mathbf{j}))}$ from (16), namely $-m_{e,\mathbf{j}}\Phi_x(x_{j_1})$, might turn zero if $m_{e,\mathbf{j}} = 0$, but since $m_{e,\mathbf{j}}$ is constant for the local equilibrium state $\mathbf{U}_{e,\mathbf{j}}$, it can be canceled by the same factor in the flux difference, so no zero divisor will occur. For isentropic steady states, the following two quantities are constant along streamlines:

$$s = \frac{p}{\rho^\gamma}, \quad Q = \frac{m^2 + n^2 + l^2}{2\rho^2} + \frac{\gamma s \rho^{\gamma-1}}{\gamma - 1} + \Phi(x).$$

Since we have assumed the equilibrium states only depend on $x$ with $n = l = 0$, the above two expressions are constant over the entire domain of computation. In addition, for such steady states we also have

$$m = \text{constant}, \quad n = 0 = \text{constant}, \quad l = 0 = \text{constant}.$$

Thus, the transformation to the equilibrium variables is defined as follows:

$$\begin{aligned}\mathbf{V}(\mathbf{U}, x) = \mathbf{V}(\rho, m, n, l, E, x) &:= (s, m, n, l, Q)^T = \left(\frac{p}{\rho^\gamma}, m, n, l, \frac{m^2 + n^2 + l^2}{2\rho^2} + \frac{\gamma s \rho^{\gamma-1}}{\gamma - 1} + \Phi(x)\right)^T \\ &= \left(\frac{\gamma - 1}{\rho^\gamma}\left(E - \frac{m^2 + n^2 + l^2}{2\rho}\right), m, n, l, (1-\gamma)\frac{m^2 + n^2 + l^2}{2\rho^2} + \frac{\gamma E}{\rho} + \Phi(x)\right)^T.\end{aligned}$$

As in the case of 2D, to compute the inverse transform $\mathbf{U} = \mathbf{U}(\mathbf{V}, x)$, the value of $(s, m, n, l, Q)$ is known, so we can first determine $\rho$ by solving the following nonlinear equation:

$$\frac{m^2 + n^2 + l^2}{2\rho^2} + \frac{\gamma s \rho^{\gamma-1}}{\gamma - 1} + \Phi(x) = Q. \tag{28}$$

Then, with this $\rho$ just obtained, $E$ can be computed from

$$E = \frac{m^2 + n^2 + l^2}{2\rho} + \frac{\rho^\gamma s}{\gamma - 1}.$$

Again, unless $\text{Mach}(\mathbf{U}) = 1$, the nonlinear equation (28) for $\rho$ has two different solutions. If $Q - \Phi(x) < \frac{\gamma+1}{2(\gamma-1)}(\gamma s)^{\frac{2}{\gamma+1}}(m^2 + n^2 + l^2)^{\frac{\gamma-1}{\gamma+1}}$, equation (28) has no solution; if $Q - \Phi(x) = \frac{\gamma+1}{2(\gamma-1)}(\gamma s)^{\frac{2}{\gamma+1}}(m^2 + n^2 + l^2)^{\frac{\gamma-1}{\gamma+1}}$, there is a unique solution with Mach $= 1$; if $Q - \Phi(x) > \frac{\gamma+1}{2(\gamma-1)}(\gamma s)^{\frac{2}{\gamma+1}}(m^2 + n^2 + l^2)^{\frac{\gamma-1}{\gamma+1}}$, there are two solutions, the smaller one corresponds to Mach $> 1$ (supersonic), and the larger one corresponds to Mach $< 1$ (subsonic). Therefore, when computing $\mathbf{U}^-\left(\mathbf{j} + \frac{1}{2}\mathbf{e}_1\right)$ and $\mathbf{U}^+\left(\mathbf{j} + \frac{1}{2}\mathbf{e}_1\right)$ for the numerical flux on the left-hand side of (16), we take the Mach number of $\mathbf{U}(\mathbf{j})$ and $\mathbf{U}(\mathbf{j} + \mathbf{e}_1)$ respectively for the inverse transform.

The construction of the local equilibrium state is exactly the same as in 2D. For any fixed $\mathbf{j} = (j_1, j_2, j_3)$, we define $\mathbf{U}_{e,\mathbf{j}}(x)$ based on the point values $\{\mathbf{U}(\mathbf{j} - 3\mathbf{e}_1), \cdots, \mathbf{U}(\mathbf{j} + 3\mathbf{e}_1)\}$ as follows:

$$\mathbf{U}_{e,\mathbf{j}}(x) = \mathbf{U}(\mathbf{V}(\rho(\mathbf{j} + \beta\,\mathbf{e}_1), m(\mathbf{j} + \beta\,\mathbf{e}_1), 0, 0, E(\mathbf{j} + \beta\,\mathbf{e}_1), x_{j_1+\beta}), x),$$

where $\beta \in \{-3, 3\}$ is the index such that $\Phi((j_1 + \beta)\Delta x)$ obtains its maximum on the interval $[(j_1 - 3)\Delta x, (j_1 + 3)\Delta x]$ (since $\Phi(x)$ is monotone, its maximum is attained at one of the end points of the interval). More precisely, let $(s_{e,\mathbf{j}}, m_{e,\mathbf{j}}, 0, 0, Q_{e,\mathbf{j}}) := \mathbf{V}(\rho(\mathbf{j} + \beta\,\mathbf{e}_1), m(\mathbf{j} + \beta\,\mathbf{e}_1), 0, 0, E(\mathbf{j} + \beta\,\mathbf{e}_1), x_{j_1+\beta})$;

then, in order to compute the local equilibrium state $\mathbf{U}_{e,\mathbf{j}}(x)$ for any $x$, we first need to solve the following equation for $\rho(x)$:

$$Q_{e,\mathbf{j}} - \Phi(x) = \frac{m_{e,\mathbf{j}}^2}{2\rho(x)^2} + \frac{\gamma \cdot s_{e,\mathbf{j}} \cdot \rho(x)^{\gamma-1}}{\gamma-1}, \tag{29}$$

and finally compute $E(x)$ from

$$E(x) = \frac{m_{e,\mathbf{j}}^2}{2\rho(x)} + \frac{\rho(x)^\gamma}{\gamma-1} s_{e,\mathbf{j}}.$$

With this choice, one can guarantee that $\mathbf{U}_{e,\mathbf{j}}(x)$ is well-defined on the interval $[(j_1-3)\Delta x, (j_1+3)\Delta x]$, since for all $x \in [(j_1-3)\Delta x, (j_1+3)\Delta x]$ we have

$$Q_{e,\mathbf{j}} - \Phi(x) \geq Q_{e,\mathbf{j}} - \Phi(x_{j_1+\beta}) \geq \frac{\gamma+1}{2(\gamma-1)} (\gamma s_{e,\mathbf{j}})^{\frac{2}{\gamma+1}} (m_{e,\mathbf{j}}^2)^{\frac{\gamma-1}{\gamma+1}},$$

so that equation (29) is always solvable. To resolve the issue that the solution to the above equation is not unique, we set the sign of Mach $-1$ to be the same as that of $\mathbf{U}(\mathbf{j}+\beta\,\mathbf{e}_1)$ when performing the inverse transform. Since $\Phi(x)$ is monotone, the sign of Mach $-1$ does not change for any essentially 1D isentropic steady state of Euler equations (see Section 2.5), so that the resulting scheme is still well-balanced.

### 2.4.3 3D Euler equations in spherical coordinates

The 3D spherical coordinate variables are denoted by $(r,\theta,\phi)$, where $r \geq 0$ is the radial distance, $\theta \in [0,\pi]$ is the polar angle, and $\phi \in [-\pi,\pi)$ is the azimuthal angle. The 3D Euler equations with gravity potential $\Phi(r,\theta,\phi)$ in conservative form and spherical coordinates can be written as follows:

$$\frac{\partial \mathbf{U}}{\partial t} + \frac{1}{r^2}\frac{\partial (r^2 \mathbf{F}_r(\mathbf{U}))}{\partial r} + \frac{1}{r\sin\theta}\frac{\partial (\sin\theta\, \mathbf{F}_\theta(\mathbf{U}))}{\partial \theta} + \frac{1}{r\sin\theta}\frac{\partial \mathbf{F}_\phi(\mathbf{U})}{\partial \phi} = \mathbf{S}(r,\theta,\phi,\mathbf{U}), \tag{30}$$

where $\mathbf{U} = (\rho, \rho u_r, \rho u_\theta, \rho u_\phi, E)^T = (\rho, m_r, m_\theta, m_\phi, E)^T$ is the vector of conservative variables, and

$$\mathbf{F}_r(\mathbf{U}) = (m_r, m_r^2/\rho + p, m_r m_\theta/\rho, m_r m_\phi/\rho, m_r(E+p)/\rho)^T, \tag{31}$$

$$\mathbf{F}_\theta(\mathbf{U}) = (m_\theta, m_r m_\theta/\rho, m_\theta^2/\rho + p, m_\theta m_\phi/\rho, m_\theta(E+p)/\rho)^T, \tag{32}$$

$$\mathbf{F}_\phi(\mathbf{U}) = (m_\phi, m_r m_\phi/\rho, m_\theta m_\phi/\rho, m_\phi^2/\rho + p, m_\phi(E+p)/\rho)^T, \tag{33}$$

$$\mathbf{S}(r,\theta,\phi,\mathbf{U}) = \begin{pmatrix} 0 \\ \frac{m_\theta^2+m_\phi^2}{\rho r} + \frac{2p}{r} - \rho\Phi_r \\ -\frac{m_r m_\theta}{\rho r} + \frac{m_\phi^2 \cot\theta}{\rho r} + \frac{p\cot\theta}{r} - \frac{\rho}{r}\Phi_\theta \\ -\frac{m_\phi(m_r + m_\theta\cot\theta)}{\rho r} - \frac{\rho}{r\sin\theta}\Phi_\phi \\ -m_r\Phi_r - \frac{m_\theta}{r}\Phi_\theta - \frac{m_\phi}{r\sin\theta}\Phi_\phi \end{pmatrix}. \tag{34}$$

In the above, $u_r$, $u_\theta$ and $u_\phi$ denote respectively the velocity in the radial, polar and azimuthal direction; $m_r := \rho u_r$, $m_\theta := \rho u_\theta$ and $m_\phi := \rho u_\phi$ denote respectively the momentum in the radial, polar and azimuthal direction. *In this paper, we only consider the situation where the potential $\Phi(r,\theta,\phi) = \Phi(r)$ is independent of $\theta,\phi$ and monotone in r, and we only attempt to preserve isentropic steady states that depend only on r, i.e. with $m_\theta = m_\phi = 0$.* Under this assumption, $\mathbf{S}(r,\theta,\phi,\mathbf{U}) = \mathbf{S}(r,\mathbf{U})$. Because of the geometric factors in spherical derivatives, the scheme (16) needs to be adapted accordingly: at the

node $\mathbf{x_j} = (r_{j_1}, \theta_{j_2}, \phi_{j_3}) = (j_1\Delta r, j_2\Delta\theta, j_3\Delta\phi)$, the scheme becomes

$$\begin{aligned}
&\frac{\mathrm{d}\mathbf{U}(\mathbf{j})}{\mathrm{d}t} + \sum_{i=1}^{3} \frac{1}{g_i(\mathbf{x_j})\Delta x_i} \left( \hat{\mathbf{F}}^{(i)}(\mathbf{U}(\mathbf{j}-2\mathbf{e}_i), \cdots, \mathbf{U}(\mathbf{j}+3\mathbf{e}_i)) - \hat{\mathbf{F}}^{(i)}(\mathbf{U}(\mathbf{j}-3\mathbf{e}_i), \cdots, \mathbf{U}(\mathbf{j}+2\mathbf{e}_i)) \right) \\
=& \frac{\mathbf{S}(r_{j_1}, \mathbf{U}(\mathbf{j}))}{\mathbf{S}(r_{j_1}, \mathbf{U}_{e,\mathbf{j}}(\mathbf{j}))} \times \\
& \sum_{i=1}^{3} \frac{1}{g_i(\mathbf{x_j})\Delta x_i} \left( \hat{\mathbf{F}}^{(i)}(\mathbf{U}_{e,\mathbf{j}}(\mathbf{j}-2\mathbf{e}_i), \cdots, \mathbf{U}_{e,\mathbf{j}}(\mathbf{j}+3\mathbf{e}_i)) - \hat{\mathbf{F}}^{(i)}(\mathbf{U}_{e,\mathbf{j}}(\mathbf{j}-3\mathbf{e}_i), \cdots, \mathbf{U}_{e,\mathbf{j}}(\mathbf{j}+2\mathbf{e}_i)) \right),
\end{aligned}$$

where $\Delta x_1 = \Delta r$, $\Delta x_2 = \Delta\theta$ and $\Delta x_3 = \Delta\phi$; $g_1(r,\theta,\phi) = r^2$, $g_2(r,\theta,\phi) = g_3(r,\theta,\phi) = r\sin\theta$; and $\hat{\mathbf{F}}^{(1)}, \hat{\mathbf{F}}^{(2)}, \hat{\mathbf{F}}^{(3)}$ are defined as in formula (13) with $\mathbf{F}$ replaced by $r^2\mathbf{F}_r, \sin\theta\,\mathbf{F}_\theta, \mathbf{F}_\phi$, respectively. Note that in the last expression, the flux difference for $i = 3$ on the right-hand side is identically zero, since $\mathbf{U}_{e,\mathbf{j}}$ is a local equilibrium state that only varies with $r$. However, the differences for $i = 1,2$ are non-zero; in the case of $i = 2$ we have

$$\begin{aligned}
&\frac{1}{r_{j_1}\sin\theta_{j_2}\Delta\theta} \left( \hat{\mathbf{F}}^{(2)}(\mathbf{U}_{e,\mathbf{j}}(\mathbf{j}-2\mathbf{e}_2), \cdots, \mathbf{U}_{e,\mathbf{j}}(\mathbf{j}+3\mathbf{e}_2)) - \hat{\mathbf{F}}^{(2)}(\mathbf{U}_{e,\mathbf{j}}(\mathbf{j}-3\mathbf{e}_2), \cdots, \mathbf{U}_{e,\mathbf{j}}(\mathbf{j}+2\mathbf{e}_2)) \right) \\
=& \left( 0, 0, \frac{2p_{e,\mathbf{j}}\cot(\theta_{j_2})}{r_{j_1}\Delta\theta} \sin\left(\frac{\Delta\theta}{2}\right) \left( 1 + \frac{118\cos\left(\frac{\Delta\theta}{2}\right) - 137\cos\left(\frac{3\Delta\theta}{2}\right) + 19\cos\left(\frac{5\Delta\theta}{2}\right)}{1920} \right), 0, 0 \right), \quad (35)
\end{aligned}$$

where $p_{e,\mathbf{j}}$ is the pressure of the local equilibrium state $\mathbf{U}_{e,\mathbf{j}}$ evaluated at the point $\mathbf{x_j}$. The only non-zero (third) component in (35) is due to the geometric factor, and can be obtained from the formula (13) with $\mathbf{F}$ replaced by $p_{e,\mathbf{j}}\sin\theta$ (note that $p_{e,\mathbf{j}}$ is constant with respect to $\theta$). The denominator in the quotient $\frac{\mathbf{S}(r_{j_1},\mathbf{U}(\mathbf{j}))}{\mathbf{S}(r_{j_1},\mathbf{U}_{e,\mathbf{j}}(\mathbf{j}))}$ can be written explicitly as

$$\mathbf{S}(r_{j_1}, \mathbf{U}_{e,\mathbf{j}}(\mathbf{j})) = (0, \frac{2p_{e,\mathbf{j}}}{r_{j_1}} - \rho_{e,\mathbf{j}}\Phi_r(r_{j_1}), \frac{p_{e,\mathbf{j}}\cot(\theta_{j_2})}{r_{j_1}}, 0, -(m_r)_{e,\mathbf{j}}\Phi_r(r_{j_1})), \quad (36)$$

where all the quantities are evaluated at the point $\mathbf{x_j}$. The third component of (36) would become zero if $\theta_{j_2} = \frac{\pi}{2}$, but this is canceled by the $\cot(\theta_{j_2})$ in the third component of (35), so that no zero divisor will occur. The fifth component might also become zero when $(m_r)_{e,\mathbf{j}}$ is zero, but since for a steady state $r^2 m_r$ is constant with respect to $r$ (see the discussion below), this too can be canceled by $r^2(m_r)_{e,\mathbf{j}}$ in the fifth component of

$$\frac{1}{r_{j_1}^2\Delta r} \left( \hat{\mathbf{F}}^{(1)}(\mathbf{U}_{e,\mathbf{j}}(\mathbf{j}-2\mathbf{e}_i), \cdots, \mathbf{U}_{e,\mathbf{j}}(\mathbf{j}+3\mathbf{e}_i)) - \hat{\mathbf{F}}^{(1)}(\mathbf{U}_{e,\mathbf{j}}(\mathbf{j}-3\mathbf{e}_i), \cdots, \mathbf{U}_{e,\mathbf{j}}(\mathbf{j}+2\mathbf{e}_i)) \right).$$

For isentropic steady states, the following two quantities are constant along streamlines:

$$s = \frac{p}{\rho^\gamma}, \quad Q = \frac{m_r^2 + m_\theta^2 + m_\phi^2}{2\rho^2} + \frac{\gamma s \rho^{\gamma-1}}{\gamma - 1} + \Phi(r).$$

Since the equilibrium states considered in this paper only depends on $r$ with $m_\theta = m_\phi = 0$, the above two expressions are constant over the entire domain of computation. In addition, for such steady states we also have

$$M := r^2 m_r = \text{constant}, \quad m_\theta = 0 = \text{constant}, \quad m_\phi = 0 = \text{constant}.$$

Thus, the transformation to the equilibrium variables is defined as follows:

$$\begin{aligned}\mathbf{V}(\mathbf{U},r) &= \mathbf{V}(\rho,m_r,m_\theta,m_\phi,E,r) := (s,M,m_\theta,m_\phi,Q)^T \\ &= \left(\frac{p}{\rho^\gamma}, r^2 m_r, m_\theta, m_\phi, \frac{m_r^2+m_\theta^2+m_\phi^2}{2\rho^2}+\frac{\gamma s\rho^{\gamma-1}}{\gamma-1}+\Phi(r)\right)^T \\ &= \left(\frac{\gamma-1}{\rho^\gamma}\left(E-\frac{m_r^2+m_\theta^2+m_\phi^2}{2\rho}\right), r^2 m_r, m_\theta, m_\phi, (1-\gamma)\frac{m_r^2+m_\theta^2+m_\phi^2}{2\rho^2}+\frac{\gamma E}{\rho}+\Phi(r)\right)^T.\end{aligned}$$

As before, to compute the inverse transform $\mathbf{U}=\mathbf{U}(\mathbf{V},r)$, the value of $(s,M,m_\theta,m_\phi,Q)$ is known. We first find $m_r = M/r^2$, then determine $\rho$ by solving the following nonlinear equation:

$$\frac{m_r^2+m_\theta^2+m_\phi^2}{2\rho^2}+\frac{\gamma s\rho^{\gamma-1}}{\gamma-1}+\Phi(r) = Q. \tag{37}$$

Then, with this $\rho$ just obtained, $E$ can be computed from

$$E = \frac{m_r^2+m_\theta^2+m_\phi^2}{2\rho}+\frac{\rho^\gamma s}{\gamma-1}.$$

The nonlinear equation (37) for $\rho$ has two different solutions unless $\mathrm{Mach}(\mathbf{U})=1$. If $Q-\Phi(r) < \frac{\gamma+1}{2(\gamma-1)}(\gamma s)^{\frac{2}{\gamma+1}}(m_r^2+m_\theta^2+m_\phi^2)^{\frac{\gamma-1}{\gamma+1}}$, equation (37) has no solution; if $Q-\Phi(r) = \frac{\gamma+1}{2(\gamma-1)}(\gamma s)^{\frac{2}{\gamma+1}}(m_r^2+m_\theta^2+m_\phi^2)^{\frac{\gamma-1}{\gamma+1}}$, there is a unique solution with $\mathrm{Mach}=1$; if $Q-\Phi(r) > \frac{\gamma+1}{2(\gamma-1)}(\gamma s)^{\frac{2}{\gamma+1}}(m_r^2+m_\theta^2+m_\phi^2)^{\frac{\gamma-1}{\gamma+1}}$, there are two solutions, the smaller one corresponds to $\mathrm{Mach}>1$ (supersonic), and the larger one corresponds to $\mathrm{Mach}<1$ (subsonic). Therefore, when computing $\mathbf{U}^-\left(\mathbf{j}+\frac{1}{2}\mathbf{e}_1\right)$ and $\mathbf{U}^+\left(\mathbf{j}+\frac{1}{2}\mathbf{e}_1\right)$ for the numerical flux on the left-hand side of (16), we take the Mach number of $\mathbf{U}(\mathbf{j})$ and $\mathbf{U}(\mathbf{j}+\mathbf{e}_1)$ respectively for the inverse transform.

For any fixed $\mathbf{j}=(j_1,j_2,j_3)$, in order to define the local equilibrium state $\mathbf{U}_{e,\mathbf{j}}(r)$, we must choose an index $\beta\in\{-3,\cdots,3\}$ such that

$$\mathbf{U}_{e,\mathbf{j}}(r) = \mathbf{U}(\mathbf{V}(\rho(\mathbf{j}+\beta\,\mathbf{e}_1), m_r(\mathbf{j}+\beta\,\mathbf{e}_1), 0, 0, E(\mathbf{j}+\beta\,\mathbf{e}_1), r_{j_1+\beta}), r)$$

is at least well-defined at the points $r = r_{j_1-3},\cdots,r_{j_1+3}$. More precisely, for any $l\in\{-3,\cdots,3\}$ set $(s_l,M_l,0,0,Q_l) := \mathbf{V}(\rho(\mathbf{j}+l\,\mathbf{e}_1), m(\mathbf{j}+l\,\mathbf{e}_1), 0, 0, E(\mathbf{j}+l\,\mathbf{e}_1), r_{j_1+l})$. Suppose an index $\beta\in\{-3,\cdots,3\}$ is chosen, then for any $r_k$ with $k=-3,\cdots,3$, we first need to solve the following equation for $\rho(r_k)$:

$$Q_\beta-\Phi(r_k) = \frac{M_\beta^2}{2r_k^4\rho(r_k)^2}+\frac{\gamma\cdot s_\beta\cdot\rho(r_k)^{\gamma-1}}{\gamma-1}, \tag{38}$$

then compute $E(r_k)$ from

$$E(r_k) = \frac{M_\beta^2}{2r_k^4\rho(r_k)}+\frac{\rho(r_k)^\gamma}{\gamma-1}s_\beta.$$

Therefore, we must choose a $\beta$ such that the nonlinear equation (38) is solvable for all $k=-3,\cdots,3$. It follows from (38) that

$$Q_\beta-\Phi(r_k) = \frac{M_\beta^2}{2r_k^4\rho(r_k)^2}+\frac{\gamma\cdot s_\beta\cdot\rho(r_k)^{\gamma-1}}{\gamma-1} \geq \frac{\gamma+1}{2(\gamma-1)}(\gamma s_\beta)^{\frac{2}{\gamma+1}}(M_\beta^2)^{\frac{\gamma-1}{\gamma+1}}r_k^{-\frac{4(\gamma-1)}{\gamma+1}}.$$

So, to formulate this problem in a different way, we set

$$A_l := \frac{\gamma+1}{2(\gamma-1)}(\gamma s_l)^{\frac{2}{\gamma+1}}(M_l^2)^{\frac{\gamma-1}{\gamma+1}} \geq 0, \quad x_l := r_l^{-\frac{4(\gamma-1)}{\gamma+1}} > 0, \quad \forall l=-3,\cdots,3.$$

Since $(s_l, M_l, 0, 0, Q_l)$ are the equilibrium variables of the known state $(\rho(\mathbf{j}+l\,\mathbf{e}_1), m(\mathbf{j}+l\,\mathbf{e}_1), 0, 0, E(\mathbf{j}+l\,\mathbf{e}_1))$, we already have

$$-A_l \cdot x_l + Q_l \geq \Phi\left(x_l^{-\frac{\gamma+1}{4(\gamma-1)}}\right), \quad \forall l = -3, \cdots, 3.$$

Now we ask for the existence of a $\beta \in \{-3, \cdots, 3\}$ such that

$$-A_\beta \cdot x_l + Q_\beta \geq \Phi\left(x_l^{-\frac{\gamma+1}{4(\gamma-1)}}\right), \quad \forall l = -3, \cdots, 3. \tag{39}$$

The next lemma shows that such $\beta$ exists only for a special class of $\Phi(\cdot)$.

**Lemma 1.** *Suppose $\Phi(\cdot)$ is monotone on $(0,\infty)$. For any real sequences $\{A_l\}_{l=-3}^3$, $\{Q_l\}_{l=-3}^3$ and $\{x_l\}_{l=-3}^3$ satisfying*

$$A_l \geq 0, \quad x_l > 0, \quad -A_l \cdot x_l + Q_l \geq \Phi\left(x_l^{-\frac{\gamma+1}{4(\gamma-1)}}\right), \quad \forall l = -3, \cdots, 3,$$

*there always exists a $\beta \in \{-3, \cdots, 3\}$ such that*

$$-A_\beta \cdot x_l + Q_\beta \geq \Phi\left(x_l^{-\frac{\gamma+1}{4(\gamma-1)}}\right), \quad \forall l = -3, \cdots, 3$$

*if and only if the function $\Phi\left(x^{-\frac{\gamma+1}{4(\gamma-1)}}\right)$ is increasing.*

*Proof.* Assume without loss of generality that $x_{-3} > \cdots, > x_3$. On the $xy$-plane, consider for $l = -3, \cdots, 3$ the lines $\mathscr{L}_l : y = -A_l \cdot x + Q_l$ and the points $\mathscr{P}_l : \left(x_l, \Phi\left(x_l^{-\frac{\gamma+1}{4(\gamma-1)}}\right)\right)$, the latter lie on the graph of $y = \Phi\left(x^{-\frac{\gamma+1}{4(\gamma-1)}}\right)$. For each $l$, the line $\mathscr{L}_l$ lies above the point $\mathscr{P}_l$. The existence of $\beta$ is equivalent to the existence of a line that lies above all points.

Since $\Phi(\cdot)$ is monotone, $\Phi\left(x^{-\frac{\gamma+1}{4(\gamma-1)}}\right)$ is also a monotone function in $x > 0$. Suppose $\Phi\left(x^{-\frac{\gamma+1}{4(\gamma-1)}}\right)$ is increasing, then by geometry the line $\mathscr{L}_{-3}$ must lie above all points since its slope is negative, so we take $\beta = -3$. However, if $\Phi\left(x^{-\frac{\gamma+1}{4(\gamma-1)}}\right)$ is decreasing, then $\mathscr{P}_3$ has the largest $y$-coordinate. One can always choose $A_l \geq 0$ and $Q_l$ such that $\mathscr{L}_l$ lies above $\mathscr{P}_l$ but below $\mathscr{P}_3$ for $l = -3, \cdots, 2$, and $\mathscr{L}_3$ lies above $\mathscr{P}_3$ but below $\mathscr{P}_{-3}$, in which case $\beta$ does not exist. ∎

It follows from the above lemma that the Newtonian potential $\Phi(r) = -\frac{G}{r}$ $(G > 0)$ does not fall into the admissible class since $\Phi\left(x^{-\frac{\gamma+1}{4(\gamma-1)}}\right)$ is decreasing. This is clearly not desirable. To resolve this issue, in the actually implementation of the scheme, whenever we could not find a $\beta \in \{-3, \cdots, 3\}$ such that (39) holds, we simply replace the right-hand side of (16) by the straightforward discretization of the source term as in the ordinary A-WENO scheme. This would not destroy the well-balanced property of the scheme, since if all the values of $\{\mathbf{U}(\mathbf{j}-3\,\mathbf{e}_1), \cdots, \mathbf{U}(\mathbf{j}+3\,\mathbf{e}_1)\}$ are from the same equilibrium state, we have $A_{-3} = \cdots = A_3$ and $Q_{-3} = \cdots = Q_3$, so that all the lines $\mathscr{L}_l$ degenerate to the same line, and therefore automatically lies above all the points; in other words, (39) would always hold if $\mathbf{U}_j$'s already form an equilibrium state. It does not destroy the capability of the scheme to capture small perturbations near the steady states either, as shown in the numerical results in Sections 3.4, 3.5 and 3.7.

Moreover, in the case of the Newtonian potential $\Phi(r) = -\frac{G}{r}$, we do not need to test (39) for all $\beta, l \in \{-3 \cdots, 3\}$. In particular, note that $\Phi\left(x^{-\frac{\gamma+1}{4(\gamma-1)}}\right) = -G \cdot x^{\frac{\gamma+1}{4(\gamma-1)}}$ is either convex $(\gamma \geq \frac{5}{3})$ or concave $(\gamma < \frac{5}{3})$. Using the notation from the proof of Lemma 1, we may simplify the two cases in the following way:

**Case 1:** Suppose $\gamma \geq \frac{5}{3}$, then $-G \cdot x^{\frac{\gamma+1}{4(\gamma-1)}}$ is convex, in which case if a line lies above $\mathscr{P}_3$ and $\mathscr{P}_{-3}$, then it is above all points. Thus, we only need to check if $\mathscr{L}_0$ lies above $\mathscr{P}_3$ and $\mathscr{P}_{-3}$:

$$-A_0 \cdot x_3 + Q_0 \geq -G \cdot x_3^{\frac{\gamma+1}{4(\gamma-1)}}, \quad -A_0 \cdot x_{-3} + Q_0 \geq -G \cdot x_{-3}^{\frac{\gamma+1}{4(\gamma-1)}}.$$

If this is true, set $\beta = 0$; otherwise use the straightforward source term discretization.

**Case 2:** Suppose $\gamma < \frac{5}{3}$, then $-G \cdot x^{\frac{\gamma+1}{4(\gamma-1)}}$ is concave. In this case, we need to check if $\mathscr{L}_0$ lies above all points except $\mathscr{P}_0$:

$$-A_0 \cdot x_l + Q_0 \geq -G \cdot x_l^{\frac{\gamma+1}{4(\gamma-1)}}, \quad l = \pm 3, \pm 2, \pm 1.$$

If this is true, set $\beta = 0$; otherwise use the straightforward source term discretization.

Note that in the above two cases, we may check for any other line instead of $\mathscr{L}_0$, but numerical experiments have shown that choosing $\mathscr{L}_0$ as the candidate is the most stable way.

## 2.5 The local adaptation step

The well-balanced scheme constructed in the previous sections is found to exhibit numerical instability near transonic regions in several 2D and 3D tests, although it generally remains stable in 1D. This is because the sign of Mach $-1$ must be chosen correctly for the inverse transform $\mathbf{V} \to \mathbf{U}$ on the cell interfaces when computing the numerical fluxes; in 1D, since the wave can only propagate either to the left or right, the sign of Mach $-1$ can be taken to be the same as that of the left or the right; in higher dimensions, the wave does not necessarily propagate along the grid lines, so the sign of Mach $-1$ is very hard to predict.

For instance, the scheme does not converge for the double Mach reflection problem, which will be discussed in Section 3.2. This happens because the distribution of super- and subsonic states is very complicated and sensitive therein, and once the sign of Mach $-1$ is not correctly determined in the inverse transform $\mathbf{V} \to \mathbf{U}$, the numerical solution will diverge from the true solution in an unstoppable manner. To make matters worse, the scheme produces large errors near the locus of sonic points even if the true solution is smooth.

To make the scheme stable, we adopt a local adaptation step before using the fifth-order WENO interpolation in the numerical flux

$$\hat{\mathbf{F}}^{(1)}(\mathbf{U}(\mathbf{j} - 2\mathbf{e}_1), \cdots, \mathbf{U}(\mathbf{j} + 3\mathbf{e}_1))$$

on the left-hand side of (16): At each cell interface $\mathbf{j} + \frac{1}{2}\mathbf{e}_1 = (j_1 + \frac{1}{2}, j_2, \cdots, j_n)$ in the $x_1$-direction, if Mach $-1$ changes sign on the set of nodes

$$\left\{ \mathbf{k} = (k_1, \cdots, k_n) : \left| k_1 - j_1 - \frac{1}{2} \right| \leq 3, |k_2 - j_2| \leq 3, \cdots, |k_n - j_n| \leq 3 \right\},$$

then we directly use WENO on the conservative variables $\mathbf{U}(\mathbf{j} - 2\mathbf{e}_1), \cdots, \mathbf{U}(\mathbf{j} + 3\mathbf{e}_1)$ on the local stencil at $\mathbf{j}$ instead of on the equilibrium variables. We do the same for

$$\hat{\mathbf{F}}^{(1)}(\mathbf{U}(\mathbf{j} - 3\mathbf{e}_1), \cdots, \mathbf{U}(\mathbf{j} + 2\mathbf{e}_1))$$

on the left-hand side of (16) with $j_1$ replaced by $j_1 - 1$. Clearly, the resulting scheme is still conservative for the subsystem of conservation laws. In 2D and 3D Cartesian coordinates, since the potential $\Phi(x)$ is assumed to be monotone, one can show that the sign of Mach $-1$ cannot change for any continuous steady state. This can be easily seen from the graph of $\psi(\rho)$ in Figure 1. At any steady state,

the graph of the function is fixed, and $Q$ is a constant. Since $\Phi(x)$ is monotone, the horizontal line with height $Q-\Phi(x)$ can either move all the way up or down as $x$ varies monotonically in the computation domain. For a continuous steady state that is transonic, the line must first reach the minimum point of $\psi(\rho)$, then move up again, which is not possible. Thus, the adaptation step does not destroy the well-balanced property of the original scheme for preserving isentropic equilibria, since they are automatically continuous.

# 3 Numerical tests

In this section, we test the performance of our well-balanced A-WENO method for Euler equations in 2D Cartesian coordinates, 3D Cartesian coordinates and spherical coordinates, respectively. For each of the three cases, we test high-order accuracy for smooth solutions, well-balanced property and capability in capturing small perturbations near equilibrium states. In all the tests, the global Lax-Friedrichs numerical flux is adopted, and the time discretization is carried out using the classical fourth-order Runge–Kutta method. Unless otherwise stated, the CFL number is taken as 0.4.

## 3.1 Accuracy tests for 1D and 2D Cartesian coordinates

We test the fifth-order accuracy of our A-WENO scheme for two analytical smooth solutions of Euler equations. First, to test the accuracy of the source term approximation, we use the 1D example considered in [23]. This is sufficient since our source term in higher dimensions is still essentially 1D, which is assumed to depend only on $x$. Taking $\Phi(x)=x$ and $\gamma=\frac{5}{3}$, then the Euler equations admit the following analytical solution:

$$\rho=1+\frac{1}{5}\sin(\pi(x-t)),\quad u=1,\quad v=0,\quad p=4.5+t-x+\frac{1}{5\pi}\cos(\pi(x-t)).$$

The computation domain is set to be $\Omega=[0,2]$, and the values of the exact solution are prescribed at the left and right end-points. The numerical solution is computed up to $t=0.1$. The number of cells are set to be $N=100,200,400,800$. We use the classical fourth order Runge-Kutta method for time discretizations with the following CFL condition of the form $\Delta t=\mathscr{O}(\Delta x^{\frac{5}{4}})$:

$$\Delta t=\frac{0.5}{\alpha}\Delta x^{\frac{5}{4}}.$$

Note that this CFL condition is only restricted to this accuracy test, and $\Delta t=\mathscr{O}(\Delta x)$ is used everywhere else. The $L^\infty$ errors of the conservative variables are shown in Table 1, demonstrating genuine fifth-order accuracy of the scheme.

Table 1: Accuracy test of traveling density wave with $\Phi(x)=x$ in 1D

| | $\rho$ | | $m$ | | $E$ | |
|---|---|---|---|---|---|---|
| $N$ | $L^\infty$ error | Order | $L^\infty$ error | Order | $L^\infty$ error | Order |
| 100 | 5.12E-07 | – | 3.43E-07 | – | 6.82E-07 | – |
| 200 | 1.09E-08 | 5.556 | 7.39E-09 | 5.537 | 1.39E-08 | 5.621 |
| 400 | 1.92E-10 | 5.828 | 1.57E-10 | 5.558 | 2.92E-10 | 5.567 |
| 800 | 3.20E-12 | 5.904 | 3.88E-12 | 5.343 | 7.30E-12 | 5.324 |

Next, we test the analytic solution known as the *isentropic vortex* for 2D Euler equations defined as follows. Set

$$X=x-x_0-u_\infty t,\quad Y=y-y_0-v_\infty t,\quad r^2=X^2+Y^2.$$

Then, the analytical solution is given by

$$u = u_\infty - \frac{\beta}{2\pi} e^{(1-r^2)/2} Y, \quad v = v_\infty + \frac{\beta}{2\pi} e^{(1-r^2)/2} X,$$
$$T = 1 - \frac{(\gamma-1)\beta^2}{8\gamma\pi^2} e^{1-r^2}, \quad \rho = T^{1/(\gamma-1)}, \quad p = T^{\gamma/(\gamma-1)}, \quad E = \frac{1}{2}\rho(u^2+v^2) + \frac{p}{\gamma-1}.$$

In the test, $x_0 = y_0 = \beta = 5$, $u_\infty = v_\infty = 2$, and the numerical solution is evolved up to $t = 0.5$ on the computation domain $\Omega = [0,10] \times [0,10]$ with boundary conditions set to be the exact solution. The number of cells in the $x$- and $y$-directions are set to be $N = N_x = N_y = 100, 200, 400, 800$, and CFL number is taken as 0.4. The $L^\infty$ errors of the conservative variables are shown in Table 2.

Table 2: Accuracy test of the isentropic vortex in 2D

| $N$ | $\rho$ | | $m$ | | $n$ | | $E$ | |
|---|---|---|---|---|---|---|---|---|
| | $L^\infty$ error | order | $L^\infty$ error | order | $L^\infty$ error | order | $L^\infty$ error | order |
| 100 | 6.05E-04 | – | 6.54E-04 | – | 1.31E-03 | – | 2.32E-03 | – |
| 200 | 3.71E-05 | 4.03 | 3.70E-05 | 4.14 | 8.06E-05 | 4.02 | 1.46E-04 | 3.99 |
| 400 | 1.93E-06 | 4.27 | 1.23E-06 | 4.91 | 3.76E-06 | 4.42 | 6.93E-06 | 4.39 |
| 800 | 4.00E-08 | 5.59 | 3.04E-08 | 5.34 | 8.29E-08 | 5.51 | 1.57E-07 | 5.46 |

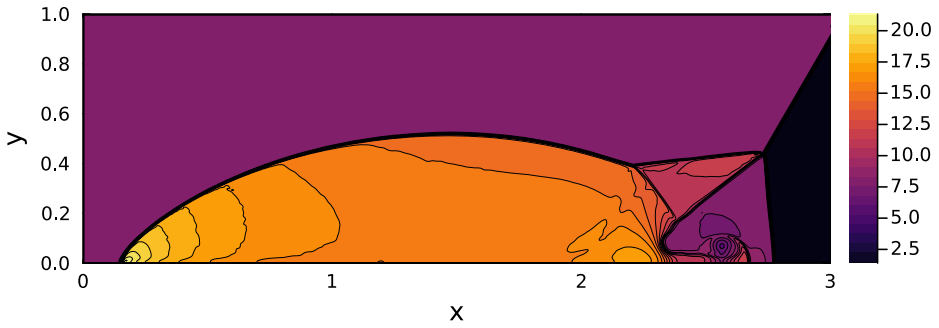
## 3.2 Double Mach reflection problem

In this test, we compute the double Mach reflection problem [19] to verify the robustness of the scheme. It involves a Mach 10 shock impinging on a reflecting wall at a 60° angle. The computation domain is $\Omega = [0,4] \times [0,1]$, with the initial condition

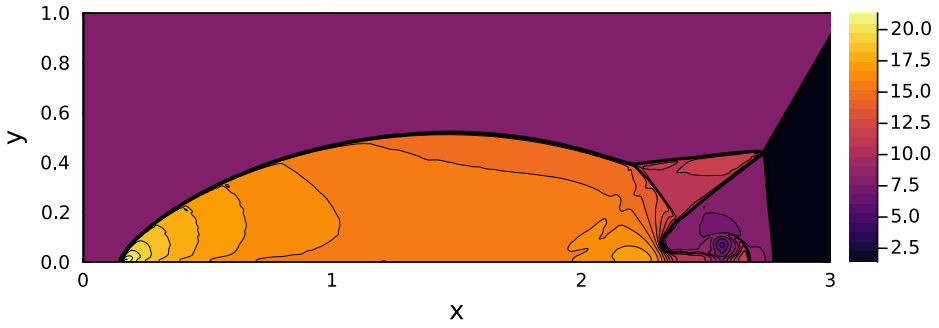
$$(\rho_0, u_0, v_0, p_0) = \begin{cases} (8, \frac{33\sqrt{3}}{8}, -\frac{33}{8}, 116.5), & \text{if } y > \sqrt{3}(x - \frac{1}{6}) \quad \text{(post-shock)} \\ (1.4, 0, 0, 1), & \text{if } y < \sqrt{3}(x - \frac{1}{6}) \quad \text{(pre-shock)}. \end{cases}$$

The inflow and outflow boundary conditions are prescribed at the left and right boundary, respectively. The top boundary values are set to equal the exact solution, which is time-dependent. On the bottom boundary, the (constant) post shock values are prescribed on the segment $\{0 \le x < \frac{1}{6}, y = 0\}$, while reflective boundary conditions are imposed on the segment $\{\frac{1}{6} < x \le 4, y = 0\}$. The numbers of cells in the $x$- and $y$-directions are $N_x = 960$ and $N_y = 240$, respectively. The numerical solution is computed up to time $t = 0.2$ using both the well-balanced A-WENO scheme and the ordinary A-WENO scheme. The computed values of $\rho$ are compared in Figure 2. No essential difference can be noted between the results of both schemes.

We also remark here that if we do not include the local adaptation stage, the well-balanced A-WENO scheme would not converge for this test. This happens because the distribution of super- and subsonic states is very complicated and sensitive near the point $(\frac{1}{6}, 0)$ at the beginning of the simulation, so that the inverse transform $\mathbf{V} \to \mathbf{U}$ would always choose the wrong branch there.




(a) The well-balanced A-WENO scheme




(b) The ordinary A-WENO scheme

Figure 2: Comparison of density computed from the well-balanced A-WENO scheme (upper) and the ordinary A-WENO scheme (lower). 30 equally spaced contour lines are distributed from 0 to 22.

### 3.3 Well-balanced tests for 2D Cartesian coordinates

We now test the well-balanced property of the A-WENO scheme for steady-state isentropic flows. Consider the examples used in [6, 23]. We use the linear potential $\Phi(x) = x$ and set $\gamma = \frac{5}{3}$. The steady state is computed by performing the inverse transform on the following constant equilibrium variables:

$$s = 1, \quad m = -\text{Mach}\,\gamma^{\frac{1}{2}}, \quad n = 0, \quad Q = \frac{1}{2}\text{Mach}^2\,\gamma + \frac{\gamma}{\gamma - 1},$$

where Mach denotes the Mach number. Clearly, since the inverse transform depends on the sign of Mach $-1$, there are in fact three cases to be tested:

**(a)** Hydrostatic flow: Mach $= 0$.

**(b)** Subsonic flow: Mach $= 0.01$.

**(c)** Supersonic flow: Mach $= 2.5$.

We compute the solution on the domain $\Omega = [0,2] \times [0,2]$ up to $t = 1$ with $N_x = N_y = 200$. Values of the exact solutions are prescribed at the left and right boundaries, while periodic boundary conditions are imposed on the upper and lower boundaries. The $L^\infty$ errors for the three cases are shown in Table 3.

Table 3: $L^\infty$ errors for different cases in the well-balanced test 3.3 with $N_x = N_y = 200$ at $t = 1$

| Case | $\rho$ | $m$ | $E$ |
|---|---|---|---|
| (a) | 2.11E-15 | 1.47E-15 | 2.66E-15 |
| (b) | 3.77E-15 | 3.50E-15 | 6.88E-15 |
| (c) | 4.73E-13 | 1.60E-12 | 3.92E-12 |

### 3.4 Small perturbation tests for 2D Cartesian coordinates

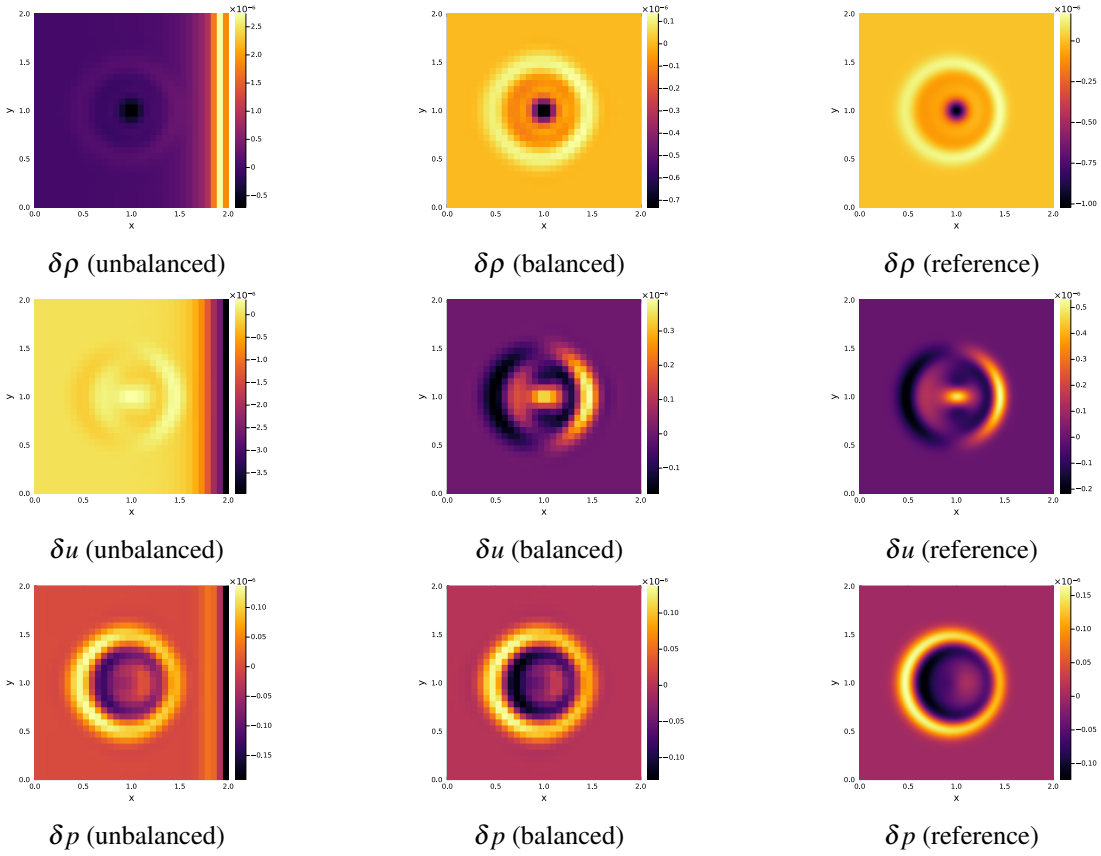
In this example, we test the capability of our well-balanced A-WENO scheme to capture small perturbation of steady states, and compare the results with those obtained from the unbalanced ordinary A-WENO scheme with a straightforward discretization of the source term. This test is a direct 2D generalization of the 1D test from [6, 23].

We add a small perturbation $\delta p_0 = A\exp(-100(x-\bar{x})^2 - 100(y-\bar{y})^2)$ on top of the initial pressure of cases (a), (b) and (c) from Section 3.3, while keeping the initial density and velocities the same. In the small perturbation tests for the three cases, $A = 10^{-6}$ and

$$\bar{x} = \bar{y} = \begin{cases} 1.0, & \text{case (a)}, \\ 1.1, & \text{case (b)}, \\ 1.5, & \text{case (c)}. \end{cases}$$

As before, the computation domain is $\Omega = [0,2]\times[0,2]$. Values of the exact solutions are prescribed at the left and right boundaries, while periodic boundary conditions are imposed on the upper and lower boundaries. The numerical solutions are computed up to $t = 0.45$, 0.45 and 0.25 for cases (a), (b) and (c) respectively. These choices of final times can guarantee that the region polluted by the perturbation stays inside $\Omega$, and no shock is formed.

The discrepancy of density, velocity and pressure with respect to their corresponding base steady states, denoted by $\delta\rho, \delta u, \delta p$, for cases (a), (b) and (c) are shown in Figures 3, 4 and 5 respectively. In each figure, the left and middle columns show the results obtained from the unbalanced and well-balanced A-WENO schemes on the coarse mesh with $N_x = N_y = 32$. The reference solutions are shown in the right column, which are computed from the well-balanced A-WENO scheme with $N_x = N_y = 200$. We can see the well-balanced scheme captures small perturbations much better than the unbalanced scheme on coarse meshes.

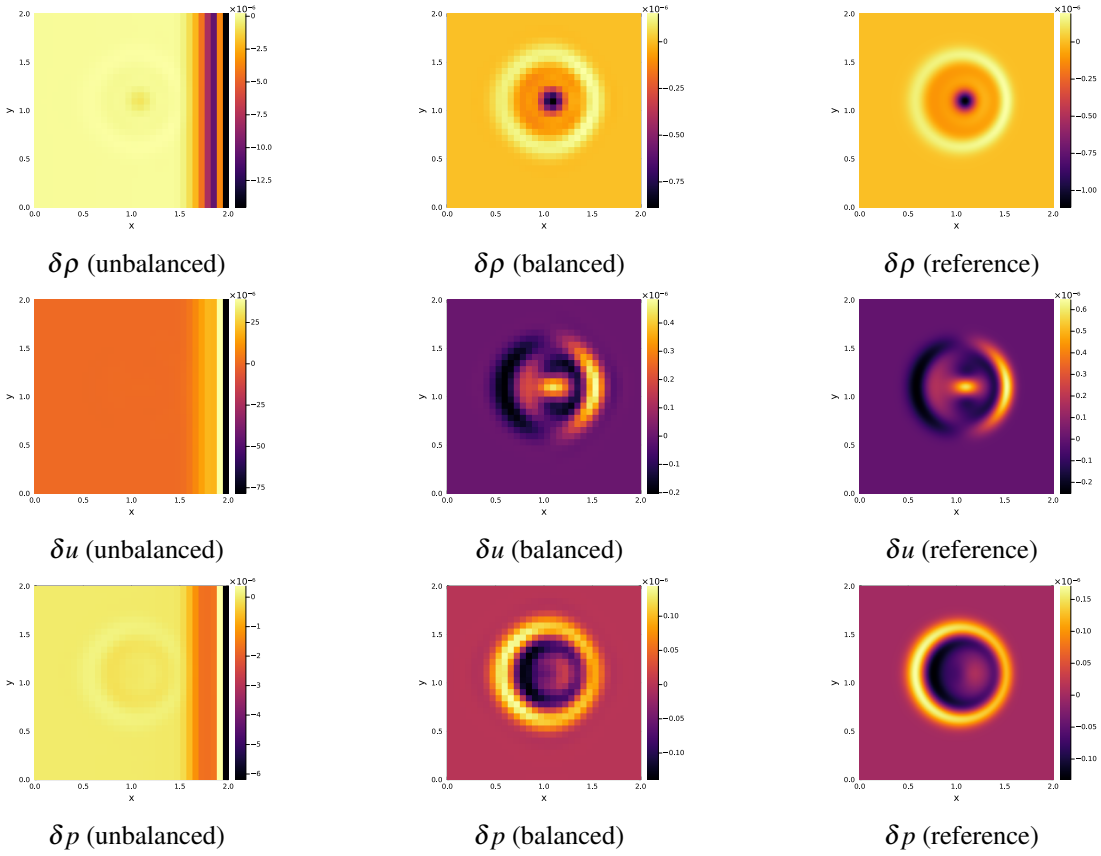


$\delta\rho$ (unbalanced) $\delta\rho$ (balanced) $\delta\rho$ (reference)

$\delta u$ (unbalanced) $\delta u$ (balanced) $\delta u$ (reference)

$\delta p$ (unbalanced) $\delta p$ (balanced) $\delta p$ (reference)

Figure 3: **Case (a)**: values of $\delta\rho, \delta u, \delta p$ computed from the ordinary A-WENO scheme (left) and the well-balanced A-WENO scheme (middle) on a coarse mesh with $N_x = N_y = 32$. The reference solution on the right is computed from the well-balanced A-WENO scheme with $N_x = N_y = 200$.



$\delta\rho$ (unbalanced) $\delta\rho$ (balanced) $\delta\rho$ (reference)

$\delta u$ (unbalanced) $\delta u$ (balanced) $\delta u$ (reference)

$\delta p$ (unbalanced) $\delta p$ (balanced) $\delta p$ (reference)

Figure 4: **Case (b)**: values of $\delta\rho, \delta u, \delta p$ computed from the ordinary A-WENO scheme (left) and the well-balanced A-WENO scheme (middle) on a coarse mesh with $N_x = N_y = 32$. The reference solution on the right is computed from the well-balanced A-WENO scheme with $N_x = N_y = 200$.

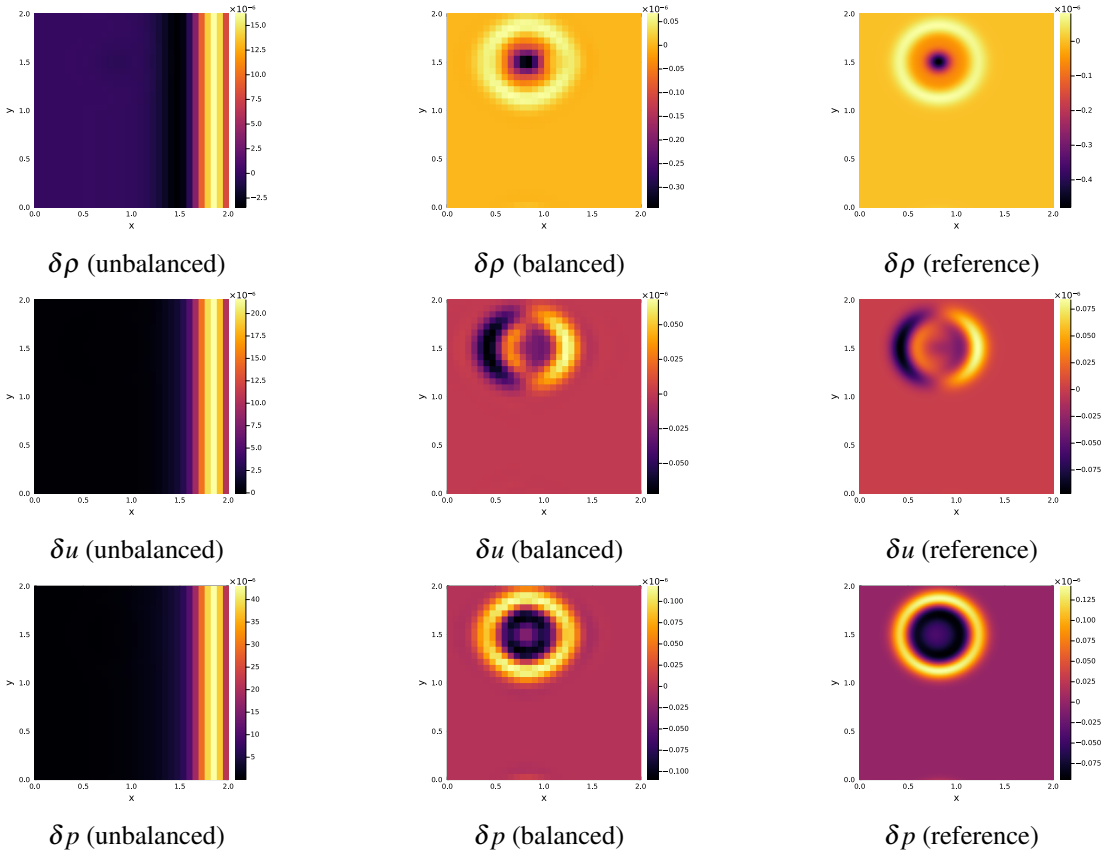



Figure 5: **Case (c)**: values of $\delta\rho, \delta u, \delta p$ computed from the ordinary A-WENO scheme (left) and the well-balanced A-WENO scheme (middle) on a coarse mesh with $N_x = N_y = 32$. The reference solution on the right is computed from the well-balanced A-WENO scheme with $N_x = N_y = 200$.

### 3.5 Small perturbation tests for 3D Cartesian coordinates

There is no need to test the well-balanced property for 3D Cartesian coordinates, because our steady states are assumed to depend only on one of the coordinates, and therefore the results in 3D would be the same as in 2D from Section 3.3. Thus, we proceed to test the capability of capturing small perturbation of steady states, and compare the results with those obtained from the unbalanced ordinary A-WENO scheme with a straightforward discretization of the source term. This test is a direct 3D generalization of the 2D test from Section 3.4.

As before, we use the linear potential $\Phi(x) = x$ and set $\gamma = \frac{5}{3}$. The steady state is computed by performing the inverse transform on the following constant equilibrium variables:

$$s = 1, \quad m = -\,\mathrm{Mach}\,\gamma^{\frac{1}{2}}, \quad n = 0, \quad l = 0, \quad Q = \frac{1}{2}\mathrm{Mach}^2\,\gamma + \frac{\gamma}{\gamma - 1},$$

where Mach denotes the Mach number. Recall that the inverse transform depends on the sign of Mach $-1$, we can therefore obtain three different steady states corresponding to three cases:

**(a)** Hydrostatic flow: Mach $= 0$.

**(b)** Subsonic flow: Mach $= 0.01$.

**(c)** Supersonic flow: Mach $= 2.5$.

Next, we add a small perturbation $\delta p_0 = A\exp(-100(x-\bar{x})^2 - 100(y-\bar{y})^2 - 100(z-\bar{z})^2)$ on top of the initial pressure in cases (a), (b) and (c), while keeping the initial density and velocities the same. In the small perturbation tests for the three cases, $A = 10^{-6}$ and

$$\bar{x} = \begin{cases} 1.0, & \text{case (a)}, \\ 1.1, & \text{case (b)}, \\ 1.5, & \text{case (c)}. \end{cases} \qquad \bar{y} = \bar{z} = 1.0.$$

The computation domain is the cube $\Omega = [0,2] \times [0,2] \times [0,2]$. Values of the exact solutions are prescribed at the faces $\{x = 0\}$ and $\{x = 2\}$, while periodic boundary conditions are imposed on the other faces. The numerical solutions are computed up to $t = 0.45$, 0.45 and 0.25 for cases (a), (b) and (c) respectively. These choices of final times can guarantee that the region polluted by the perturbation stays inside $\Omega$, and no shock is formed.

The discrepancy of density, velocity and pressure with respect to their corresponding base steady states, denoted by $\delta\rho, \delta u, \delta p$, for cases (a), (b) and (c) are shown in Figures 6, 7 and 8 respectively. In each figure, we show the numerical solutions on the planes $\{x = 1\}$, $\{y = 1\}$ and $\{z = 1\}$. The left and middle columns show the results obtained from the unbalanced and well-balanced A-WENO schemes on the coarse mesh with $N_x = N_y = N_z = 31$. The reference solutions are shown in the right column, which are computed from the well-balanced A-WENO scheme with $N_x = N_y = N_z = 127$. We can see the well-balanced scheme captures small perturbations much better than the unbalanced scheme on coarse meshes.

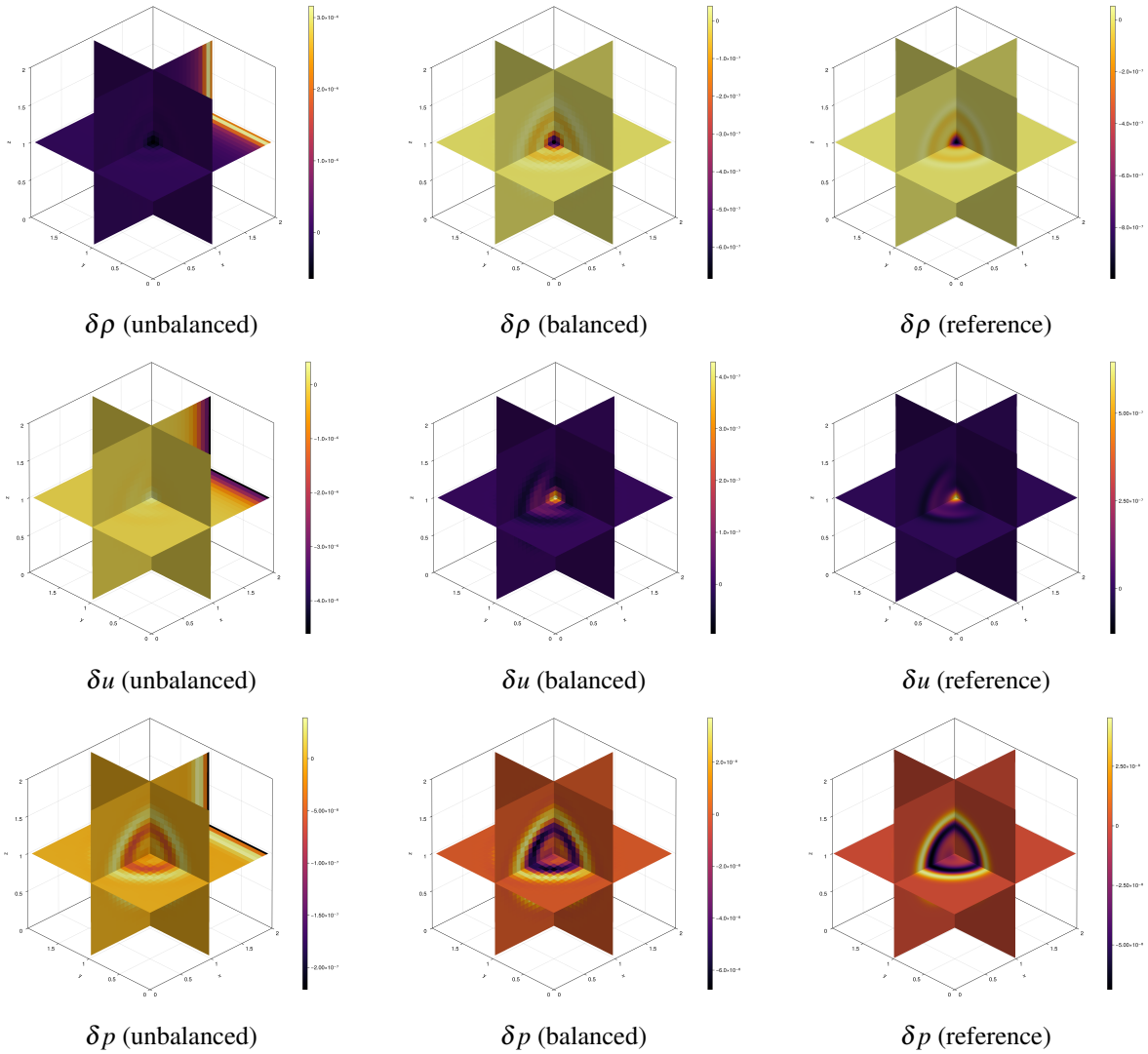
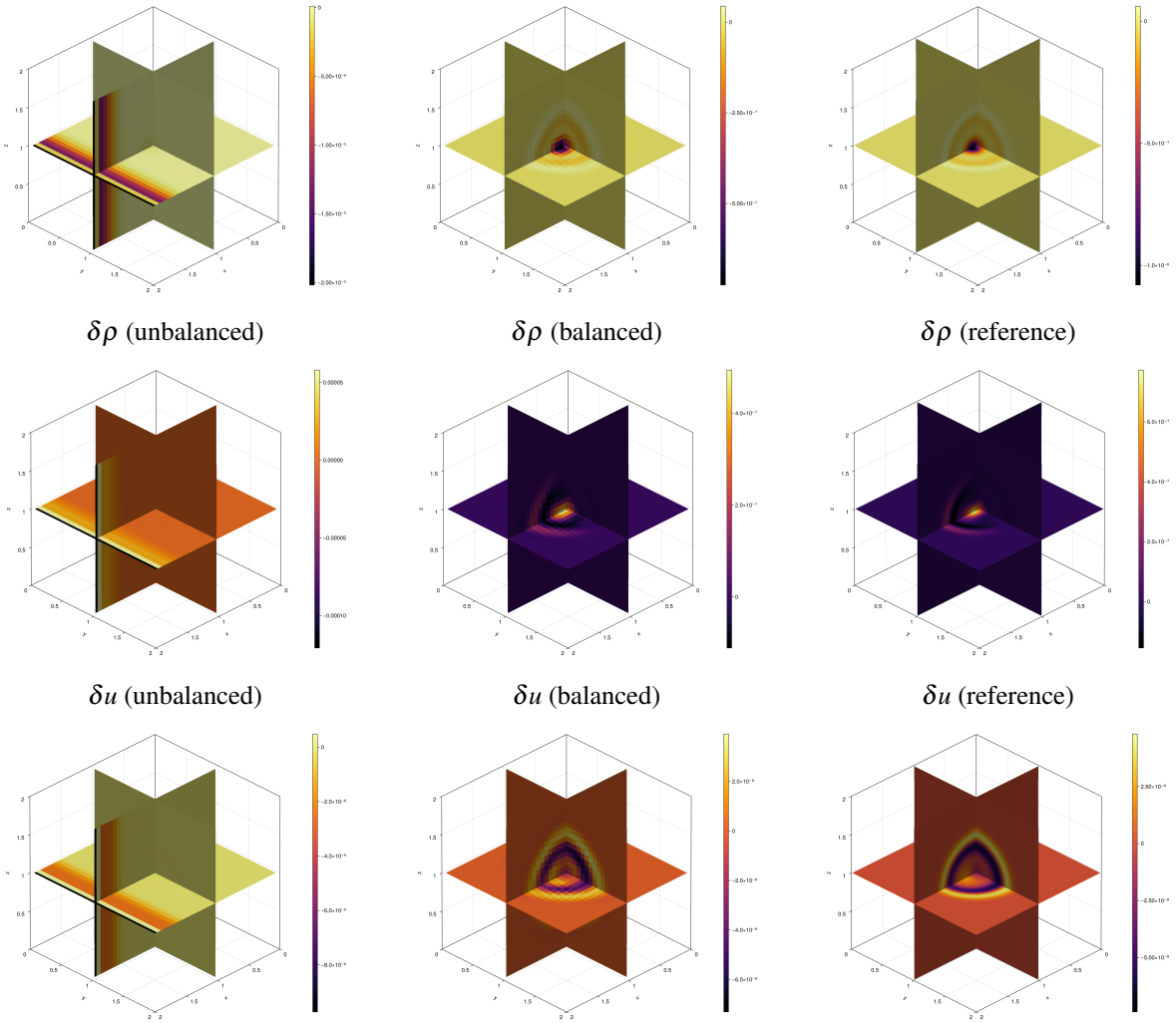



Figure 6: **Case (a)**: values of $\delta\rho, \delta u, \delta p$ computed from the ordinary A-WENO scheme (left) and the well-balanced A-WENO scheme (middle) on a coarse mesh with $N_x = N_y = N_z = 31$. The reference solution on the right is computed from the well-balanced A-WENO scheme with $N_x = N_y = N_z = 127$.



$\delta\rho$ (unbalanced) $\delta\rho$ (balanced) $\delta\rho$ (reference)

$\delta u$ (unbalanced) $\delta u$ (balanced) $\delta u$ (reference)

$\delta p$ (unbalanced) $\delta p$ (balanced) $\delta p$ (reference)

Figure 7: **Case (b)**: values of $\delta\rho, \delta u, \delta p$ computed from the ordinary A-WENO scheme (left) and the well-balanced A-WENO scheme (middle) on a coarse mesh with $N_x = N_y = N_z = 31$. The reference solution on the right is computed from the well-balanced A-WENO scheme with $N_x = N_y = N_z = 127$.

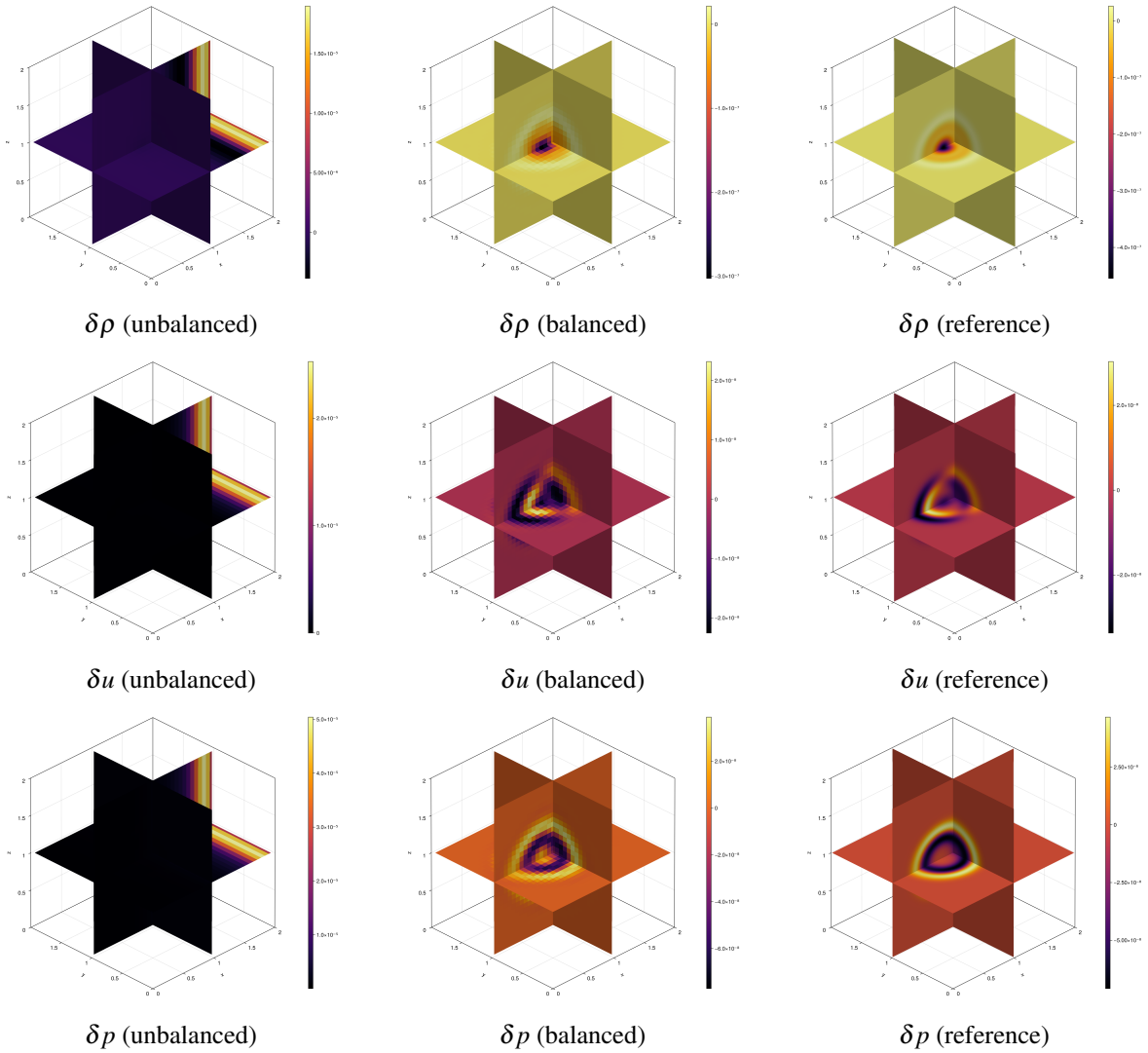



Figure 8: **Case (c)**: values of $\delta\rho, \delta u, \delta p$ computed from the ordinary A-WENO scheme (left) and the well-balanced A-WENO scheme (middle) on a coarse mesh with $N_x = N_y = N_z = 31$. The reference solution on the right is computed from the well-balanced A-WENO scheme with $N_x = N_y = N_z = 127$.

### 3.6 Well-balanced test for 3D spherical coordinates

We now test the well-balanced property of the A-WENO scheme for Euler equations in 3D spherical coordinates. This is the 3D generalization of the 1D examples used in [6]. The steady states are spherically symmetric and describe the accretion of gas onto a star, commonly known as Bondi accretion flows. Let $\Phi(r) = -\frac{1}{r}$ and set $\gamma = \frac{4}{3}$. For a generic spherically symmetric steady state $(\rho(r), m_r(r), 0, 0, E(r))$, the continuity equation and radial momentum equation in (30) simplify to

$$u_r \frac{\mathrm{d}\rho}{\mathrm{d}r} + \rho \frac{\mathrm{d}u_r}{\mathrm{d}r} + \frac{2\rho u_r}{r} = 0, \quad u_r \frac{\mathrm{d}u_r}{\mathrm{d}r} + \frac{1}{\rho}\frac{\mathrm{d}p}{\mathrm{d}r} = -\frac{\mathrm{d}}{\mathrm{d}r}\Phi(r).$$

Using the relation $c^2 = \frac{\mathrm{d}p}{\mathrm{d}\rho}$ (where $c$ denotes the speed of sound), the above equations further simplify to

$$\left(u_r - \frac{c^2}{u_r}\right)\frac{\mathrm{d}u_r}{\mathrm{d}r} = \frac{2c^2}{r} - \frac{\mathrm{d}}{\mathrm{d}r}\Phi(r) = \frac{2c^2}{r} - \frac{1}{r^2}.$$

Therefore, if the steady state is transonic, then at the sonic point $r_0$ we must have both $u_{r,0}^2 = c_0^2$ and $\frac{2c_0^2}{r_0} = \frac{1}{r_0^2}$, the latter implies $c_0^2 = \frac{1}{2r_0}$. Thus, it would be easier to define the steady state by the values of density, radial velocity and speed of sound at the reference point $r_0 = 1$:

$$\rho_0 = 1, \quad c_0^2 = \frac{1}{2} = \frac{1}{2r_0}, \quad u_{r,0} = -\,\mathrm{Mach}\, c_0,$$

where Mach denotes the Mach number. It follows that as long as Mach $\neq 1$, the steady state thus defined is either entirely subsonic or entirely supersonic. We test the following two cases:

**(a)** Subsonic flow: Mach $= 0.9$.

**(b)** Supersonic flow: Mach $= 2.0$.

The computation domain is $[R_0, R_1] \times [\frac{\pi}{4}, \frac{3\pi}{4}] \times [-\frac{\pi}{4}, \frac{\pi}{4}]$, where $R_0 = 0.2$, $R_1 = 1.8$. The solutions are computed up to $t = 0.1$ with $N_r = N_\theta = N_\phi = 32$. Values of the exact solutions are prescribed at all boundaries. The $L^\infty$ errors for the two cases are shown in Table 4.

Table 4: $L^\infty$ errors for different cases in the well-balanced test 3.6 with $N_r = N_\theta = N_\phi = 32$ at $t = 0.1$

| Case | $\rho$ | $m_r$ | $m_\theta$ | $m_\phi$ | $E$ |
|---|---|---|---|---|---|
| (a) | 8.17E-14 | 3.85E-13 | 1.06E-13 | 1.12E-13 | 3.41E-13 |
| (b) | 2.66E-13 | 6.50E-13 | 2.11E-13 | 2.14E-13 | 1.57E-12 |

### 3.7 Small perturbation tests for 3D spherical coordinates

In this example, we test the capability of our well-balanced A-WENO scheme to capture small perturbation of steady states in 3D spherical coordinates, and compare the results with those obtained from the unbalanced ordinary A-WENO scheme with a straightforward discretization of the source term. This test is a direct 3D generalization of the 1D test from [6].

We add a small perturbation $\delta p_0 = A\exp(-((r-\bar{r})^2 + (\theta-\bar{\theta})^2 + (\phi-\bar{\phi})^2)/\sigma^2)$ on top of the initial pressure of cases (a) and (b) from Section 3.6, while keeping the initial density and velocities the same. In the following tests for the two cases, $A = 10^{-4}$, $\sigma = 0.08$ and

$$\bar{r} = 0.4R_0 + 0.6R_1, \quad \bar{\theta} = \frac{\pi}{2}, \quad \bar{\phi} = 0.$$

The computation domain is still $[R_0, R_1] \times [\frac{\pi}{4}, \frac{3\pi}{4}] \times [-\frac{\pi}{4}, \frac{\pi}{4}]$, with $R_0$ and $R_1$ the same as in Section 3.6. Values of the exact solutions are prescribed at all boundaries. The numerical solutions are computed up to

$$t = 0.5 \min \left( 0.6 \frac{R_1 - R_0}{c_0 + |u_{r,0}|}, 0.3 \frac{R_1 - R_0}{\max(c_0 - |u_{r,0}|, 10^{-10})} \right).$$

This choice of final time can guarantee that the region polluted by the perturbation stays inside $\Omega$, and no shock is formed. The discrepancy of density, radial velocity and pressure with respect to their corresponding base steady states, denoted by $\delta\rho, \delta u_r, \delta p$, for cases (a) and (b) are shown in Figures 9 and 10 respectively, where only the values on the section $\theta = \frac{\pi}{2}$ is drawn. In each figure, the left and middle columns show the results obtained from the unbalanced and well-balanced A-WENO schemes on the coarse mesh with $N_r = N_\theta = N_\phi = 31$. The reference solutions are shown in the right column, which are computed from the well-balanced A-WENO scheme with $N_r = N_\theta = N_\phi = 127$. We can see the well-balanced scheme captures small perturbations much better than the unbalanced scheme on coarse meshes.

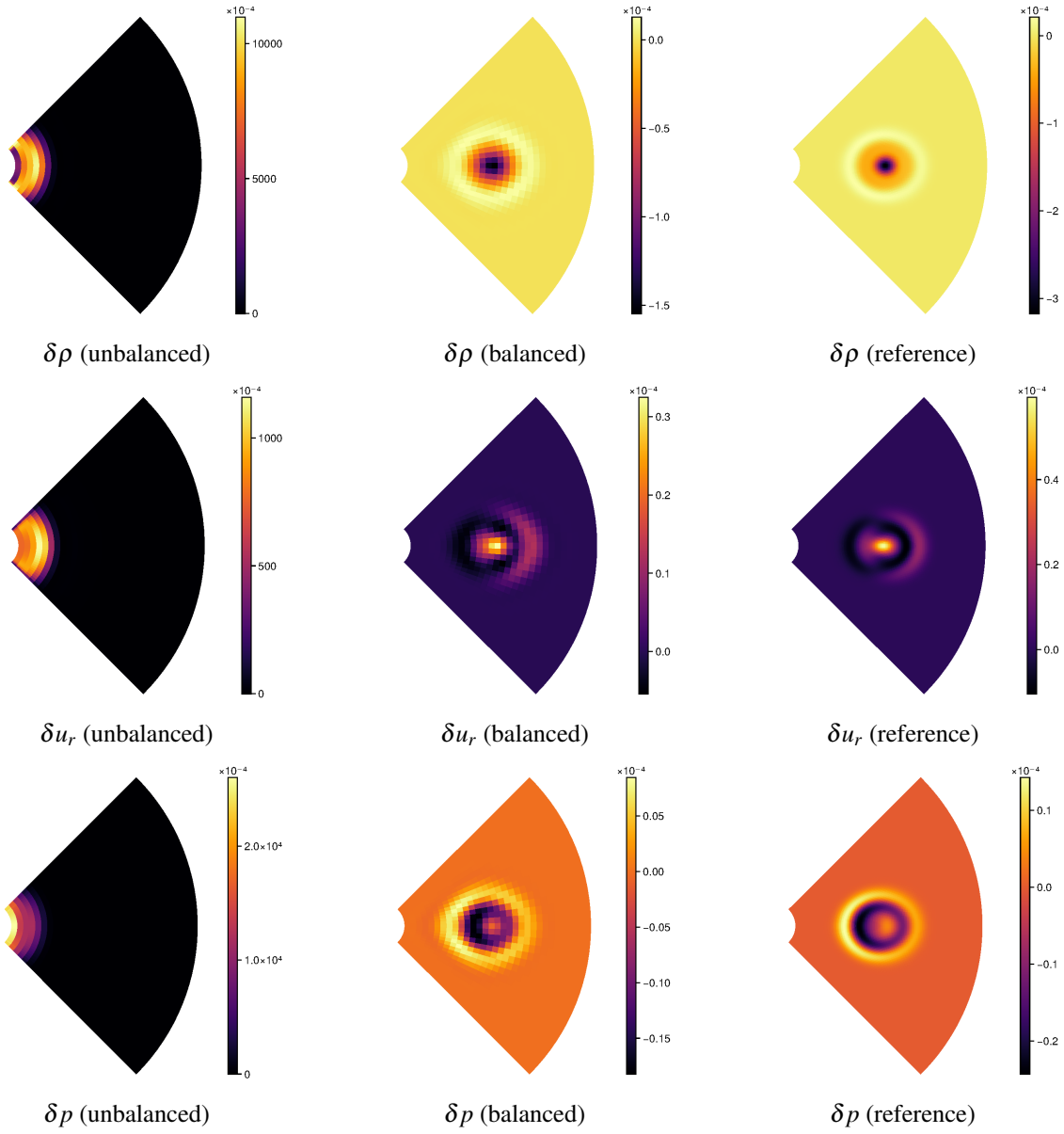



Figure 9: **Case (a)**: values of $\delta\rho, \delta u_r, \delta p$ computed from the ordinary A-WENO scheme (left) and the well-balanced A-WENO scheme (middle) on a coarse mesh with $N_r = N_\theta = N_\phi = 31$. The reference solution on the right is computed from the well-balanced A-WENO scheme with $N_r = N_\theta = N_\phi = 127$.

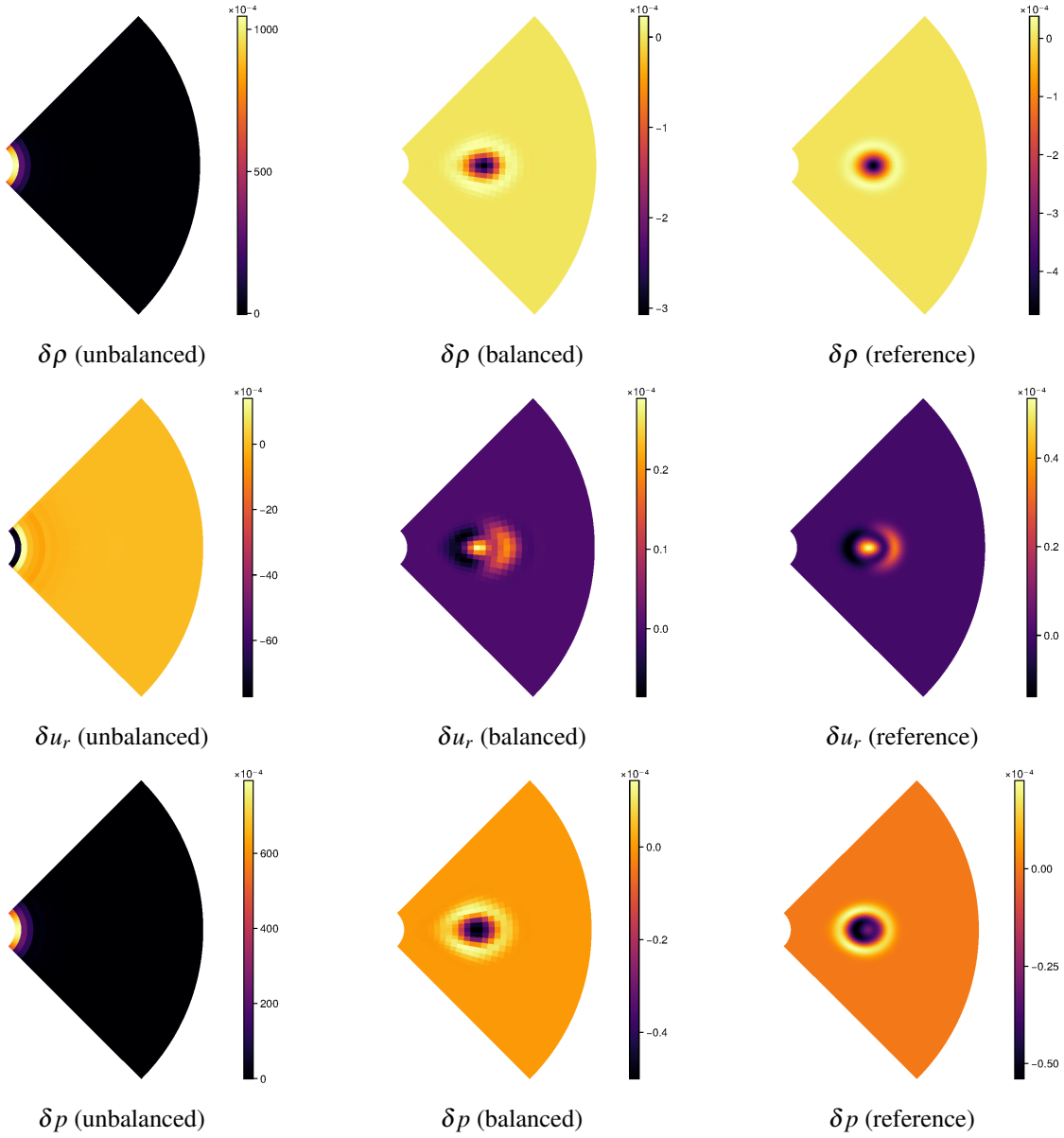



Figure 10: **Case (b)**: values of $\delta\rho, \delta u_r, \delta p$ computed from the ordinary A-WENO scheme (left) and the well-balanced A-WENO scheme (middle) on a coarse mesh with $N_r = N_\theta = N_\phi = 31$. The reference solution on the right is computed from the well-balanced A-WENO scheme with $N_r = N_\theta = N_\phi = 127$.

### 3.8 Discontinuous wave propagation in 3D spherical coordinates

To test the robustness of the scheme, we enlarge the perturbation in Section 3.7 by taking $A = 100$ in the initial pressure deviation $\delta p_0$, while keeping all the other parameters the same. Cases (a) and (b) from Section 3.7 are tested with this new initial condition. To ensure that the solution develops into a shock wave before the end of the simulation, the final time is now defined as

$$t = 0.08 \min\left(0.6\frac{R_1 - R_0}{c_0 + |u_{r,0}|}, 0.3\frac{R_1 - R_0}{\max(c_0 - |u_{r,0}|, 10^{-10})}\right).$$

The computation domain is the same as in Section 3.7, but the number of cells is taken to be $N_r = N_\theta = N_\phi = 127$. We compare the results obtained from the well-balanced A-WENO scheme and the unbalanced A-WENO scheme in Figures 11 and 12, where only the values on the section $\theta = \frac{\pi}{2}$ is drawn. The test for case (a) using the well-balanced scheme is obtained by setting CFL $= 0.3$, while all the others use CFL $= 0.4$.

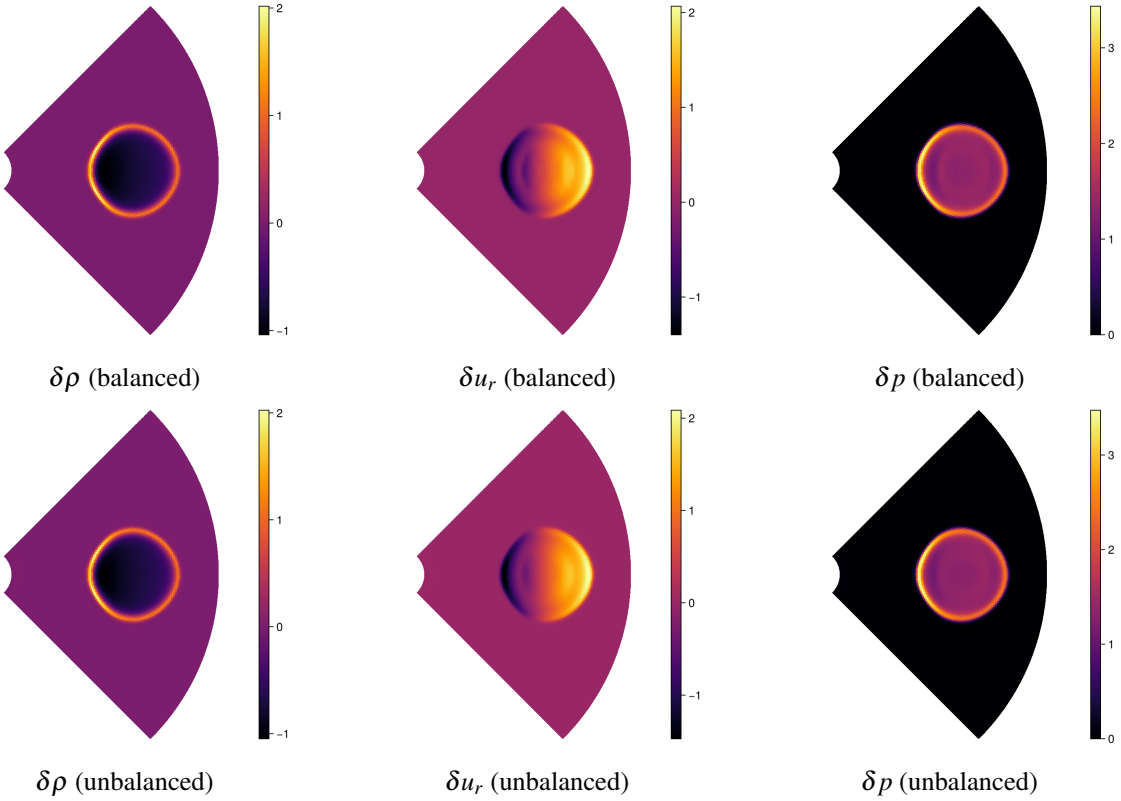



Figure 11: **Case (a)**: values of $\delta\rho, \delta u_r, \delta p$ computed from the well-balanced A-WENO scheme (upper) and the ordinary A-WENO scheme (lower) on the mesh $N_r = N_\theta = N_\phi = 127$.

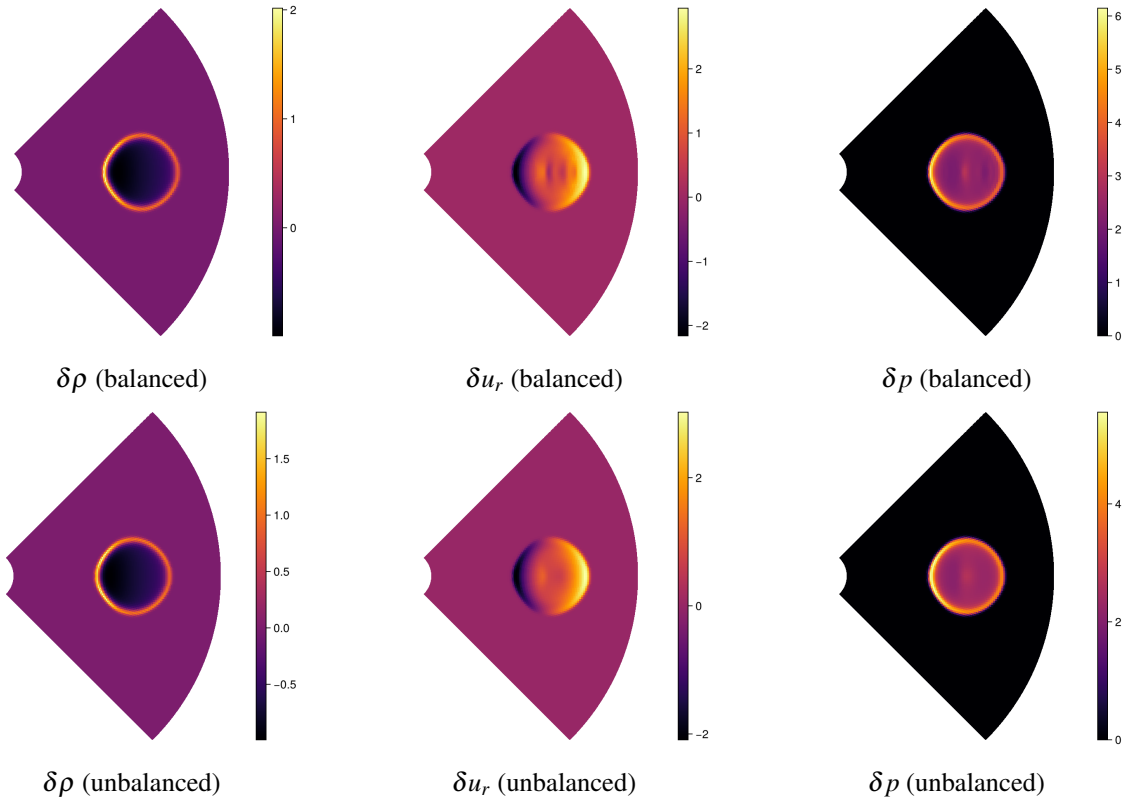



Figure 12: **Case (b)**: values of $\delta\rho, \delta u_r, \delta p$ computed from the well-balanced A-WENO scheme (upper) and the ordinary A-WENO scheme (lower) on the mesh $N_r = N_\theta = N_\phi = 127$.

# 4 Concluding Remarks

In this paper, we have developed a conservative high-order well-balanced A-WENO method for the Euler equations with gravitational source terms. The proposed method is designed to exactly preserve a class of isentropic steady states, including both hydrostatic and non-hydrostatic equilibria. The well-balanced property is achieved by reformulating the source terms using local reference equilibrium states and performing WENO interpolation on suitably chosen equilibrium variables. The use of the A-WENO framework allows the resulting scheme to maintain both high-order accuracy and the conservation property.

The method has been extended to multidimensional Euler equations in Cartesian and spherical coordinates. In particular, the treatment of spherical coordinates incorporates the geometric source terms into the well-balanced formulation. Numerical experiments have verified the designed high-order accuracy and demonstrated that the targeted steady states are preserved up to round-off errors. The proposed method also accurately resolves small perturbations of equilibrium states, even on extremely coarse meshes, and remains robust for problems away from equilibrium.

The present work focuses on steady states that are one-dimensional in nature. The development of high-order well-balanced A-WENO methods for more general multidimensional equilibria, as well as further extensions to other systems of hyperbolic balance laws, will be considered in future work.

# References

[1] P. Cargo and A. Y. LeRoux. Un schéma équilibre adapté au modèle d'atmosphère avec termes de gravité. *C. R. Acad. Sci. Paris*, 318(1):73–76, 1994.

[2] E. Carlini, R. Ferretti, and G. Russo. A weighted essentially nonoscillatory, large time-step scheme for Hamilton–Jacobi equations. *SIAM Journal on Scientific Computing*, 27(3):1071–1091, 2005.

[3] P. Chandrashekar and M. Zenk. Well-balanced nodal discontinuous Galerkin method for Euler equations with gravity. *Journal of Scientific Computing*, 71:1062–1093, 2017.

[4] Y. Cheng and A. Kurganov. Moving-water equilibria preserving central-upwind schemes for the shallow water equations. *Communications in Mathematical Sciences*, 14:1643–1663, 2016.

[5] J. M. Greenberg and A. Y. LeRoux. A well-balanced scheme for the numerical processing of source terms in hyperbolic equations. *SIAM Journal on Numerical Analysis*, 33(1):1–16, 1996.

[6] L. Grosheintz-Laval and R. Käppeli. Well-balanced finite volume schemes for nearly steady adiabatic flows. *Journal of Computational Physics*, 423:109805, 2020.

[7] A. Harten, B. Engquist, S. Osher, and S. R. Chakravarthy. Uniformly high order accurate essentially non-oscillatory schemes, III. *Journal of Computational Physics*, 71(2):231–303, 1987.

[8] G.-S. Jiang and C.-W. Shu. Efficient implementation of weighted ENO schemes. *Journal of Computational Physics*, 126(1):202–228, 1996.

[9] R. Käppeli. Well-balanced methods for computational astrophysics. *Living Reviews in Computational Astrophysics*, 8:2, 2022.

[10] R. Käppeli and S. Mishra. Well-balanced schemes for the Euler equations with gravitation. *Journal of Computational Physics*, 259:199–219, 2014.

[11] C. Klingenberg, G. Puppo, and M. Semplice. Arbitrary order finite volume well-balanced schemes for the Euler equations with gravity. *SIAM Journal on Scientific Computing*, 41(2): A695–A721, 2019.

[12] R. J. LeVeque. Balancing source terms and flux gradients in high-resolution Godunov methods: The quasi-steady wave-propagation algorithm. *Journal of Computational Physics*, 146(1):346–365, 1998.

[13] G. Li and Y. Xing. Well-balanced discontinuous Galerkin methods for the Euler equations under gravitational fields. *Journal of Scientific Computing*, 67:493–513, 2016.

[14] G. Li and Y. Xing. Well-balanced finite difference weighted essentially non-oscillatory schemes for the Euler equations with static gravitational fields. *Computers & Mathematics with Applications*, 75:2071–2085, 2018.

[15] S. Noelle, Y. Xing, and C.-W. Shu. High-order well-balanced finite volume WENO schemes for shallow water equation with moving water. *Journal of Computational Physics*, 226:29–58, 2007.

[16] C. Parés and C. Parés-Pulido. Well-balanced high-order finite difference methods for systems of balance laws. *Journal of Computational Physics*, 425:109880, 2021.

[17] P. Roe. Approximate Riemann solvers, parameter vectors, and difference schemes. *Journal of Computational Physics*, 43(2):357–372, 1981.

[18] K. Sebastian and C.-W. Shu. Multidomain WENO finite difference method with interpolation at subdomain interfaces. *Journal of Scientific Computing*, 19(1-3):405 – 438, 2003.

[19] P. Woodward and P. Colella. The numerical simulation of two-dimensional fluid flow with strong shocks. *Journal of Computational Physics*, 54(1):115–173, 1984.

[20] K. Wu and Y. Xing. Uniformly high-order structure-preserving discontinuous Galerkin methods for Euler equations with gravitation: Positivity and well-balancedness. *SIAM Journal on Scientific Computing*, 43:A472–A510, 2021.

[21] Y. Xing. Exactly well-balanced discontinuous galerkin methods for the shallow water equations with moving water equilibrium. *Journal of Computational Physics*, 257:536–553, 2014.

[22] Y. Xing and C.-W. Shu. High order well-balanced WENO scheme for the gas dynamics equations under gravitational fields. *Journal of Scientific Computing*, 54:645–662, 2013.

[23] Z. Xu and C.-W. Shu. A high-order well-balanced discontinuous Galerkin method for hyperbolic balance laws based on the Gauss-Lobatto quadrature rules. *Journal of Scientific Computing*, 101 (2):39, 2024.

[24] Z. Xu and C.-W. Shu. A well-balanced conservative high-order alternative finite difference WENO (A-WENO) method for the shallow water equations. *Advances in Water Resources*, 196:104898, 2025.